Electronic Supplementary Information

Hypoxia Active Cyclometalated Ir(III) Nile Red Triplet Photosensitisers

Judit Fodor,[a] Olga Mazuryk,[b] Claire C. Condon,[a] Oriol Careta,[c] Amani B. Al Riyami,[a] Carme Nogués,[c] John J. Colleran,[d] Jianzhang Zhao,[e] Sylvia M. Draper*[a]*

[a] *School of Chemistry, Trinity College Dublin, College Green, Dublin 2, Ireland*
[b] *Department of Inorganic Chemistry, Faculty of Chemistry, Jagiellonian University, Gronostajowa 2, 30-387, Krakow, Poland*
[c] *Departament de Biologia Cellular, Fisiología i Immunologia, Universitat Autònoma de Barcelona, E-08193 Bellaterra, Barcelona, Spain.*
[d] *Central Quad Grangegorman, School of Chemical and Pharmaceutical Sciences, Technological University Dublin, Dublin 7, D07 H6K8 Dublin, Ireland*
[e] *State Key Laboratory of Fine Chemicals, Frontier Science Center for Smart Materials, Dalian University of Technology, E208 Western Campus, 2 Ling-Gong Road, Dalian 116012, P. R. China*

Table of Contents

Experimental

All reagents and chemicals used in the synthetic procedures were purchased from Sigma Aldrich, Acros Organics (Fisher Scientific) and Fluorochem, and were used without further purification. Reactions were carried out in an inert atmosphere Ar using standard Schlenk techniques unless stated otherwise. Solvents were dried using appropriate drying agents and distilled under a nitrogen atmosphere. Flash chromatography was performed using silica gel 60 (Sigma Aldrich/Merck), particle size 40-63 μm. Thin-layer chromatography (TLC) was performed using Merck 60 F254 silica gel (pre-coated, 0.2 mm thick, 20 x 20 cm) and visualised by UV light (λmax 254 nm).

1.1 General Methods

Photophysical Measurements: All photophysical studies were carried out with solutions contained in 1x1 cm quartz cells in HPLC grade solvents. Where appropriate, deaerated solutions were obtained using specialised freeze-pump-thaw degassing cuvettes, and the solutions were subjected to at least three freeze-pump-thaw cycles. UV-vis absorption spectra were recorded on a Shimadzu UV-2450 and/or Varian, Cary 50 Scan UV-visible spectrophotometers. Emission and excitation spectra, and emission quantum yields were recorded on a Horiba FluoroMax-4 spectrofluorometer and/or on a Varian Cary Eclipse spectrofluorometer. Emission quantum yields of solutions were measured using the single-point relative method, using $[Ru(bpy)_3](PF_6)_2$ (for **[Ir-2ENR]PF_6** and **[Ir-3ENR]PF_6**) or Nile Red (for **2ENR** and **3ENR**) as the reference, in MeCN at RT. Emission lifetime measurements were performed on a Horiba-Jobin-Yvon FluoroLog FL-3-11 spectrofluorometer with a TBX-04-D picosecond photodetection module using a NanoLED pulsed diode laser excitation sources (λ_{ex} = 460 nm).

Mass Spectroscopy: Electrospray ionisation (ESI) mass spectra were recorded on a micromass LCT electrospray mass spectrometer, or a Bruker MicrOTOF-Q-III mass spectrometer. Accurate MS were referenced against leucine enkephalin (555.6 g mol^{-1}) or [Glu1]-Fibrinopeptide B (1570.6 g mol^{-1}) and were reported within 5 ppm. MALDITOF mass spectra were recorded on a Waters MALDI-QTOF Premier spectrometer using an α-cyano4-hydroxy cinnamic acid matrix.

NMR Spectroscopy: ^{1}H NMR, $^{13}C\{1H\}$ NMR, ^{31}P NMR, and ^{19}F NMR spectra were recorded using a Bruker Advance DPX400 MHz, Bruker AV-400 MHz, or Bruker AV-600 MHz spectrometer in $CDCl_3$, $(CD_3)_2SO$ or CD_3CN with tetramethylsilane as the internal standard. ^{13}C NMR spectra are proton decoupled and reported as $^{13}C\{1H\}$. PSYCHE pure shift NMR spectroscopy aided the assignment of the ^{1}H NMR spectra of **[Ir-2ENR]PF_6** and **[Ir-3ENR]PF_6**, which suppressed the effects of homonuclear coupling and produced ^{1}H NMR spectra with chemical shifts only, showing no multiplicity.

Electrochemistry: The electrochemical measurements were performed with a CH Instruments, Inc. (IJ Cambria Scientific Ltd., Llanelli, UK) potentiostat, model 620A. Pt working (2 mm diameter, from CH Instruments, Inc.), non-aqueous $Ag/AgNO_3$ reference (BAS Inc., West Lafayette, IN, USA) electrodes and a platinum wire (from Surepure Chemetals, Florham Park, NJ, USA) counter electrode were used for the measurements. The supporting electrolyte was 0.1 M tetrabutylammonium hexafluorophosphate ($TBAPF_6$) in acetonitrile.

1.2 Singlet Oxygen Quantum Yields

The singlet oxygen quantum yields of the complexes were measured standard (Φ_Δ = 83 % in CH_2Cl_2) in CH_3CN, λ_{ex} = 534 nm, and with methylene blue as the standard (Φ_Δ = 57 % in CH_2Cl_2) in CH_3CN, λ_{ex} = 610 nm. and 1,3-diphenylisobenzofuran (DPBF) as the $^1O_2$ scavenger. The absorbance of DPBF at λ 410 nm was adjusted to 1.0 in air-saturated acetonitrile. The absorption of the photosensitiser was adjusted to between 0.2 and 0.3 at the excitation wavelength (λ_{ex} 534/610 nm). After addition of the photosensitiser to the cuvette, the peak absorption of the solution was determined every 20 s on irradiation with mono-chromatic light. The slope of the absorption at λ 410 nm was calculated by plotting the absorption changes versus the photoirradiation time, and the Φ_Δ was determined by the equation below:

$$\Phi_{\Delta unk} = \Phi_{\Delta ref} \times \frac{k_{unk}}{k_{ref}} \times \frac{F_{unk}}{F_{ref}} \times \left(\frac{\eta_{unk}}{\eta_{ref}}\right)^2 \quad \text{(eq. 1)}$$

where *unk* and *ref* are the unknown sample and standard reference compound respectively. k is the slope of the plotted absorption peak values at λ 410 nm in the solution. F is the absorption correction factor, which is given by $F = 1–10^{-O.D.}$; and O. D. is the optical density of the solution at the irradiation wavelength and η is the refractive indices of the sample and the reference.

1.3 Nanosecond Time-Resolved Transient Absorption

Nanosecond time-resolved transient absorption spectra were recorded at Dalian University of Technology and were measured on a LP980 laser flash photolysis spectrometer (Edinburgh Instruments, UK). All samples used in the laser flash photolysis experiments were deaerated with N_2 for ~15 minutes before measurement, and the gas flow was kept constant during the measurement. The lifetime values (by monitoring the decay trace of the transients) were obtained with the LP900 software.

1.4 Cell Culture – SKBR-3 cells

Experiments were conducted with SKBR-3 cells, a tumorigenic human mammary epithelial cell line (ATCC, USA). Cells were cultured and maintained in McCoy's 5A modified medium (Gibco, UK) supplemented with 10% foetal bovine serum (Gibco) in a 37 °C humidified incubator set to 5 % CO_2 (standard culture conditions). For Alamar Blue Cytotoxicity assay (Thermo Fisher Scientific) viability experiments, cells were seeded in 24-well plates at a density of 3.5×10^4 cells per well. For confocal laser scanning microscopy, cells were seeded in special confocal 35 mm dishes provided glass coverslip bottom (μ-Dish 35 mm, high Glass Bottom, Ibidi, DE) at a density of 1.75×10^5 cells per dish. All treatments were performed 24 h after seeding. To add the PS to the cultures, stock solutions were prepared in pure DMSO (Sigma/Aldrich) to a final concentration of 1 mM, and then diluted in McCoy's 5A modified medium supplemented with 10 % FBS), obtaining a final compound concentration of 0.01, 0.05, 0.1, 0.5, 1, 2.5, 5 and 10 and 1 μM and a maximum of 1 % of DMSO in the cultures.

1.4.1 Alamar Blue Assay

Before testing the effect of photodynamic treatment on cell viability, the toxicity of the PSs in dark conditions (dark toxicity) was evaluated. SKBR-3 cells (35,000 cells/well) were seeded in fresh medium and incubated in the dark for 24 h. Subsequently, the medium was replaced with medium containing the PS at different concentrations and incubated for an additional 24 h. After this incubation, the medium was removed, and the cells were washed with Hank's Balanced Salt Solution (HBSS) to remove any non-internalised PS. Fresh medium was added to the cells. The cell viability was then tested with the Alamar Blue assay (24 h). The cells were incubated for an additional 48 h (in absence of PS), and a second Alamar Blue assay was performed (72 h). The timeline for testing the dark toxicity of the PSs is summarised in Fig. S21.

1.4.2 Photodynamic Treatments

SKBR-3 cells were incubated without (control) or with 0.01 and 0.05 μM of **[Ru-2ENR]Cl_2** and 0.01 μM of **[Ru-3ENR]Cl_2** for 4 h. Then, cells were washed with HBSS and fresh medium was added. Cells were then either kept in dark conditions (Not irradiated) or irradiated for 15 min using a PhotoActivation Universal Light device (PAUL, GenIUL), in the range of 620–630 nm (red light) and with a mean intensity of 55 $mWcm^{-2}$ (light dose of 33 Jcm^{-2}). After photodynamic treatment, cell culture viability assessments were performed. Again, one right after irradiation (4 h) and another one after being incubated (in absence of PS) for an additional 48 h in standard conditions (52 h), using the Alamar Blue Assay. Three independent experiments were performed for each condition.

1.4.3 Product Internalisation

Product internalisation experiments were then performed with SKBR-3 cells to analyse the cellular uptake of the different PSs. After 24 h of cell seeding, 10 μM of product was added to the culture. 4h after product incubation in standard conditions in the dark, cells were washed four times with HBSS to remove non internalized product and incubated with 5 μL of Wheat germ agglutinin (WGA) 448 for 15 min to detect the limit of the cells. Then, images were acquired with a Leica TCS-SP5 AOBS spectral Confocal Laser Scanning Microscope (Leica Microsystems) using a PlanApochromatic 63X objective lens. WGA-Alexa Fluor 488 (plasma membrane) and product excitation was carried out using a 488 nm laser line in both cases, using a sequential mode. Different PMT devices (580-699 nm for product fluorescence emission and 500-535 nm for Wheat Germ Agglutinin (WGA) fluorescence emission (membrane)) were used to detect each corresponding spectral range. Series of images were further analysed with Fiji software (NIH, Maryland, USA).

1.5 Cell Culture – MCF-7 cells

MCF-7 cell line was cultured and maintained in MEM medium (Corning) supplemented with 10% foetal bovine serum (EurX), 1 % of penicillin-streptomycin solution (Corning), 2 mM glutamine (Corning) and 1% of non-essential amino acids (Corning) in a 37 °C humidified incubator set to 5 % CO_2. Hypoxic conditions were maintained in a humidified hypoxic chamber (Coy) filled with a gas mixture comprising 94% N_2, 5 % CO_2, and 1% O_2. For tests under hypoxic conditions, cells were seeded under normal oxygen concentration and then transferred to hypoxic conditions for at least 24 h preincubation. The

medium intended to be used in hypoxic experiments was also preincubated in the hypoxic chamber for at least 24 h.

1.5.1 Cytotoxicity and phototoxicity assays

For cyto- and phototoxicity experiments, cells were seeded in 96-well plates at a density of 3 × 10^4 cells per well 24 h prior to the experiments. Stock solutions of Ir(III) complex were added to wells in basal medium and incubated for desired period of time. DMSO concentration was kept constant at 0.5% in all experiments. The viability of cells was determined using the resazurin assay. Resazurin is a blue, non-fluorescent dye that upon reduction by metabolically active cells produces a pink, highly fluorescent product. The test was performed by incubating treated cells with resazurin sodium salt dissolved in Dulbecco's phosphate-buffered saline with Ca^{2+} and Mg^{2+} (DPBS, 50 μM) for 1.5 h. The amount of fluorescent resorufin was quantified at 605 nm (using 560 nm excitation wavelength) bya Tecan Infinite 200 microplate reader. The IC_{50} values were determined using the Hill equation (eq.1, OriginPro2018). The effect of the compound in the dark was denoted as IC_{50}^{dark}, while the effect in the dark and under hypoxic conditions IC_{50}^{hyp}.

$$y = y_0 + \frac{(y_{100} - y_0)[c]^H}{[IC_{50}]^H + [c]^H} \quad \text{(eq. 2)}$$

For phototoxic studies, cells were incubated with Ir(III) complex at non-toxic concentrations ($<IC_{50}^{dark}/2$) for 24 h and then washed with DPBS and irradiated with monochromatic green wavelength 520 nm for 5 min (82 mJ cm^{-2}, 273.2 μWcm^{-2}). After the irradiation, cells were kept in the fresh complete medium for 24 h, after which the viability assay was performed. The IC_{50} values obtained upon irradiation were denoted as IC_{50}^{hv}.

1.5.2 [Ir-3ENR]Cl accumulation

The accumulation of the compound was measured using inductively coupled plasma mass spectrometry ICP-MS. MCF-7 cells were seeded on 6 wells plates a the density of 3.5×10^4 cells per cm^2 a day before the experiment. Next, cells were incubated with various concentrations of the [Ir-3ENR]Cl for 24 h. To correctly measure the accumulation of Ir only non-toxic concentrations were used. Additional attention was paid to eliminate dead cells by washing the cells' monolayer with PBS. The incubated cells were washed, detached by trypsin treatment, counted, and centrifuged. The supernatant was removed, and the cells were digested in concentrated nitric acid overnight at room temperature. Subsequently, the solutions were diluted with Millipore water to a final nitric acid concentration of 10%. The results were expressed as Ir concentration per cell.

For fractionation experiments, MCF-7 cells were seeded on 6 wells plates with a density of 3.5×10^4 cells per cm^2 a day before the experiment. Next, cells were incubated with 2 μM [Ir-3ENR]Cl for 24 h The incubated cells were washed, detached by trypsin treatment, counted, and centrifuged. The fractionation was done using Subcellular Protein Fractionation Kit for Cultured Cells (Thermofisher Scientific) according to the manufacturer's instructions. Solutions were digested in concentrated nitric acid overnight at room temperature and subsequently analyzed by ICP-MS.

1.5.3 ROS generation

For evaluation of ROS production *in vitro*, MCF-7 cells were seeded on 96-well plates with a density of 3×10^4 cells per cm^2. Ir(III) complex was added at non-toxic concentrations and incubated for 24 h. After that, the compound was washed, and cells were incubated with different fluorescent probes for different amount of time (20 µM DCFDA 30 min; 5 µM HPF 30 min; 10 µM HE 30 min; 10 µM Mitosox 30 min, 10 µM Bodipy C581/591 C11 (Lipid peroxidation sensor) 30 min, 5 µM SOSG 2h). After the staining, probes were washed with PBS twice and the fluorescence intensity of the cells was quantified by a Tecan Infinite 200 plate reader using the following excitation/emission wavelengths: 485/535 nm for DCFDA, HPF, and SOSG and 520/605 nm for HE, Mitosox. To measure the photogeneration of ROS, the cells were further irradiated with 520 nm light (82 mJ cm^{-2}, 273.2 µWcm^{-2}) after staining with fluorescent probes. Part of the plates was covered to obtain dark control cells. Next, the fluorescence of the cells was quantified as described earlier.

For scavenger experiments, MCF-7 cells were seeded on 96-well plates with a density of 6×10^4 cells per cm^2. Ir(III) complex in the presence of NAC (5 mM), NaN3 (2 mM), or D-mannitol (50 mM) was added and incubated for 24 h under normoxic or hypoxic conditions. After that ROS generation or viability of cells were measured respectively with DCFDA assay or with resazurin test. For photoactivated measurements, ROS generation was measured directly after the irradiation DCF-loaded cells co-incubated with [Ir-3ENR]Cl and ROS scavengers, while viability was measured 24 h ahter the irradiation. The fluorescence of the cells was quantified as described earlier.

1.5.4 [Ir-3ENR]Cl localisation

For co-localization experiments, MCF-7 cells were seeded in 96-well plates at a density of 3×10^4 cells per well 24 h prior to the experiment. Mitotracker Green (Life Technologies) was used to image mitochondria according to the manufacturer's protocols. **[Ir-3ENR]Cl** was incubated in basic medium for 24 h (1 µM), then rinsed twice with PBS. Images were acquired using an Olympus fluorescence microscope IX83.

1.6 Statistical analysis

The statistical analysis of the results was performed using GraphPad Prism version 8.01 for Windows, (GraphPad Software, La Jolla, California, USA). Quantitative results were analysed using one-way ANOVA with a minimal significance level set at $P \leq 0.05$. In the figures, significance is represented with an asterisk, which means that the values are significantly different from their control ($p < 0.05$).

Synthesis

3-([2,2'-bipyridin]-5-ylethynyl)-9-(diethylamino)-5*H*-benzo[*a*]phenoxazin-5-one; **3ENR-bpy**

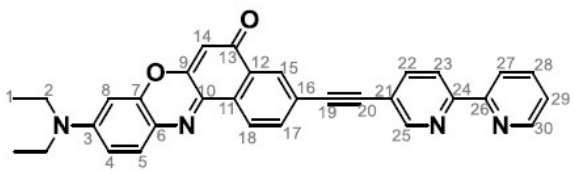

3ENR (0.05 g, 0.15 mmol), 5-Br-2,2'-bpy (0.052 g, 0.22 mmol) and $Pd(PPh_3)_4$ (0.025 g,

0.02 mmol) were dissolved in MeCN (5 mL) and Et_3N (5 mL) and the reaction mixture was heated to 80 ˚C for 24 h under Ar. The solvent was evaporated *in vacuo* and the crude product purified *via* column chromatography (silica, toluene, EtOAC, 1:1 v/v) to yield **3ENR-bpy** as a dark purple solid (0.012 g, 17 %).

δH (DMSO-d_6, 600 MHz, 25 ˚C): 8.95 (d, $^4J_{HH}$ 1.5 Hz, 1H, H-25), 8.73 (d, $^3J_{HH}$ 4.5 Hz, 1H, H-30), 8.63 (d, $^3J_{HH}$ 8.2 Hz, 1H, H-18), 8.47 (d, $^3J_{HH}$ 8.0 Hz, 1H, H-23), 8.43 (d, $^3J_{HH}$ 7.9 Hz, 1H, H-27), 8.31 (d, $^4J_{HH}$ 1.6 Hz, 1H, H-15), 8.21 (dd, $^3J_{HH}$ 8.2, $^4J_{HH}$ 2.1 Hz, 1H, H-22), 8.02 – 7.96 (m, 2H, H-17, H-28), 7.67 (d, $^3J_{HH}$ 9.1 Hz, 1H, H-5), 7.50 (td, $^3J_{HH}$ 6.0 Hz, $^4J_{HH}$ 1.1 Hz, 1H, H-29), 6.90 (dd, $^3J_{HH}$ 9.1, $^4J_{HH}$ 2.7 Hz, 1H, H-4), 6.73 (d, $^4J_{HH}$ 2.6 Hz, 1H, H-8), 6.35 (s, 1H, H-14), 3.54 (q, $^3J_{HH}$ 6.9 Hz, 4H, H-2), 1.18 (t, $^3J_{HH}$ 7.0 Hz, 6H, H-1) ppm.

δC (DMSO-d_6, 151 MHz, 25 ˚C): 181.08, 154.46, 154.35, 151.67, 149.56, 146.72, 139.93, 137.54, 133.79, 124.68, 124.04, 122.85, 120.94, 120.12, 110.85, 104.52, 96.09, 44.60, 12.49 ppm (Sample poorly soluble common deuterated organic solvents for full $^{13}C\{^1H\}$ characterisation, therefore $^{13}C\{^1H\}$ spectral data is incomplete).

HRMS (m/z, ESI$^+$, MeOH) [M+H]+ $(C_{32}H_{25}N_4O_2)^+$ Calculated mass: 497.1972; Found 497.1973.

UV visible absorption (MeCN): λ_{abs} (Ɛ) 560 nm (61,700 M^{-1} cm^{-1}).

Emission (MeCN): λ_{em} 635 nm (λ_{ex} 560 nm).

[Ir(2-phenylpyridine)2(5-bromo-2, 2'-bipyridine)]PF_6; **Ir1**

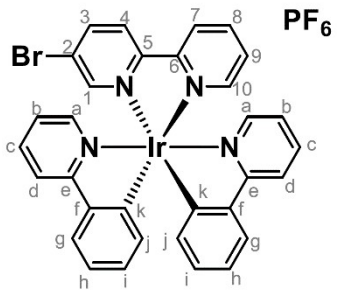

Ir0 (0.046 g, 0.043 mmol) and **5-Br-2,2'-bpy** (0.02 g, 0.085 mmol) were dissolved in CH_2Cl_2 (5 mL), and heated to 40 ˚C overnight. Upon cooling, a saturated solution of NH_4PF_6 in MeOH was added dropwise to the reaction mixture. The precipitate was filtered and washed with deionised water and diethyl ether to yield **Ir1** as an orange solid (0.055 g, 73 %).

δH (CD_3CN, 600 MHz, 25 ˚C): 8.49 (d, $^3J_{HH}$ 8.1 Hz, 1H, H-7), 8.42 (d, $^3J_{HH}$ 8.7 Hz, 1H, H-4), 8.29 (d, $^3J_{HH}$ 8.8 Hz, 1H, H-3), 8.12 (t, $^3J_{HH}$ 7.9 Hz, 1H, H-8), 8.08-8.05 (m, 2H, H-d), 7.97 (d, $^3J_{HH}$ 5.4 Hz, 1H, H-10), 7.93 (s, 1H, H-1), 7.88-7.84 (m, 2H, H-c), 7.82-7.79 (m, 2H, H-g), 7.68 (d, $^3J_{HH}$ 5.8 Hz, 1H, H-a), 7.58 (d, $^3J_{HH}$ 5.8 Hz, 1H, H-a), 7.52 (t, $^3J_{HH}$ 6.6 Hz ,1H, H-9), 7.10-7.01 (m, 4H, H-b, H-h), 6.93 (m, 2H, H-i), 6.29 (d, $^3J_{HH}$ 7.6 Hz, 1H, H-j), 6.24 (d, $^3J_{HH}$ 7.6 Hz, 1H, H-j) ppm.

δC (CD_3CN, 151 MHz, 25 ˚C): 168.22 (CQ, C-e), 168.11 (CQ, C-e), 155.90 (CQ, C-6), 155.74 (CQ, C-5), 152.35 (CH, C-10), 151.67 (CH, C-1), 150.65 (CQ, C-k), 150.52 (CH, C-a), 150.27 (CQ, C-k), 150.24 (CH, C-a), 145.10 (CQ, C-f), 144.92 (CQ, C-f) , 142.82 CH, C-3), 140.36 (CH, C-8), 139.61 (CH, C-c), 139.57 (CH, C-c), 132.56 (CH, C-j), 132.35 (CH, Cj), 131.39 (CH, C-i), 131.33 (CH, C-i), 129.62 (CH, C-9), 126.60 (CH, C- 4), 125.90 (CH, 2C, C-7, C-g), 125.83 (CH, C-g), 125.36 (CQ, C-2), 124.56 (CH, C-b), 124.44 (CH, C-b), 123.74 (CH, C-h), 123.63 (CH, C-h), 121.00 (CH, C-d), 120.81 (CH, C-d) ppm.

HRMS (m/z, MALDI-TOF, MeOH) $[M-PF_6]^+$ $(C_{32}H_{23}N_4BrIr)^+$ Calculated mass: 735.0736; Found: 735.0729.

[Ir(2-phenylpyridine)2(5-(3ENR)-2, 2'-bipyridine)]PF_6; **[Ir-3ENR]PF_6**

Off-the-complex synthesis: **Ir0** (0.008 g, 0.007 mmol) **3ENR-bpy** (0.007 g, 0.0141 mmol) were dissolved in $CHCl_3$ (0.5 mL), and heated to 60 ˚C overnight. Upon cooling, a saturated solution of NH_4PF_6 in MeOH was added dropwise to the reaction mixture. The solvent was evaporated in vacuo and the crude product purified via column chromatography (silica, CH_2Cl_2, MeOH 99:1 v/v) to yield **[Ir-3ENR]PF_6** as a purple solid (0.009 g, 58 %).

On-the-complex synthesis: **Ir1** (0.05 g, 0.06 mmol), **3ENR** (0.05 g, 0.15 mmol) and $Pd(PPh_3)_4$ (0.007 g, 0.006 mmol) were dissolved in MeCN (2.5 mL) and Et_3N and the reaction mixture was heated to 80 ˚C for 24 h under Ar. The solvent was evaporated *in vacuo* and the crude product purified *via* column chromatography (silica, MeCN, H_2O, KNO_3 100:10:1 v/v/v) followed by treatment with KPF_6 to yield **[Ir-3ENR]PF_6** as a dark purple solid (0.023 g, 36 %).

δH (CD_3CN, 600 MHz, 25 ˚C): 8.60 (d, $^3J_{HH}$ 8.3 Hz, 1H, H-18), 8.55-8.52 (m, 2H, H-23, H-27), 8.28-2.27 (m, 2H, H-15, H-22), 8.14 (t, $^3J_{HH}$ 7.6 Hz, 1H, H-28), 8.10-8.06 (m, 3H, H-25, H-34, H-49), 7.99 (t, $^3J_{HH,}$ 5.6 Hz, 1H, H-30), 7.88-7.84 (m, 3H, H-33, H-37, H-50), 7.81 (d, $^3J_{HH}$ 9.0 Hz, 1H, H-45), 7.78 (dd, $^3J_{HH}$ 8.3 Hz, $^4J_{HH}$ 1.6 Hz, H-17), 7.73 (d, $^3J_{HH}$ 5.8 Hz, 1H, H-52)7.61-7.60 (m, 2H, H-31, H-5), 7.51 (t, $^3J_{HH}$ 6.6 Hz, 1H, H-29), 7.09 (t, $^3J_{HH}$ 6.6 HZ, 1H, H-38), 7.07-7.03 (m, 3H, H-44, H-51, H-32), 6.97 (t, $^3J_{HH}$ 7.5 Hz, 1H, H-39), 6.93 (t, $^3J_{HH}$ 7.4 Hz, 1H, H-43), 6.83 (dd, $^3J_{HH}$ 9.1 Hz, $^4J_{HH}$ 2.6 Hz, 1H, H-4), 6.58 (d, $^4J_{HH}$ 2.6 Hz, 1H, H-8), 6.32 (d, $^3J_{HH}$ 7.5 Hz, 1H, H-40), 6.29 (s, 1H, H-14), 6.27 (d, $^3J_{HH}$ 7.3 Hz, 1H, H-42), 3.52 (q, $^3J_{HH}$ 7.1 Hz, 4H, H-2), 1.22 (t, $^3J_{HH}$ 7.1 Hz, 6H, H-1) ppm.

δC (CD_3CN, 151 MHz, 25 ˚C): 182.54 (CQ, C-13), 168.44 (CQ, C-35), 168.27 (CQ, C-48), 156.19 (CQ, C-26), 155.93 (CQ, C-24), 154.02 (CQ, C-9), 153.34 (CH, C-25), 152.75 (CQ, C-3), 151.80 (CH, C-30), 150.85 (CQ, C-41), 150.70 (CQ, C-47), 150.57 (CH, C-52), 150.30 (CH, C-31), 148.12 (CQ, C-7), 145.15 (CQ, C-36), 145.03 (CQ, C-46), 142.41 (CH, C-22), 140.36 (CH, C-28), 139.65 (CH, C-33), 139.62 (CH, C-50), 138.88 (CQ, C-10), 134.62 (CH, C-17), 133.82 (CQ, C-11), 132.64 (CH, C-40), 132.60 (CQ, C-12), 132.44 (CH, C-5), 132.37 (CH, C-37), 131.52 (CH, C-39), 131.41 (CH, C-43), 129.96 (CH, C- 15), 129.61 (CH, C-29), 126.13 (2C, C-27, C-6), 126.05 (CH, C-37), 125.91 (CH, C-45), 125.41 (CH, C-23), 125.29 (CQ, C-21), 124.98 (CH, C-18), 124.57 (CH, C-32), 124.54 (CH, C-51), 123.77 (CH, C-38), 123.68 (CH, C-44), 123.21 (CQ, C-16), 121.06 (CH, C- 34), 120.90 (CH, C-49), 111.67 (CH, C-4), 105.65 (CH, C-14), 97.04 (CH, C-8), 96.97 (CQ, C-19), 86.98 (CQ, C-20), 45.89 (CH2, 2C, C-2), 12.82 (CH3, 2C, C-1) ppm.

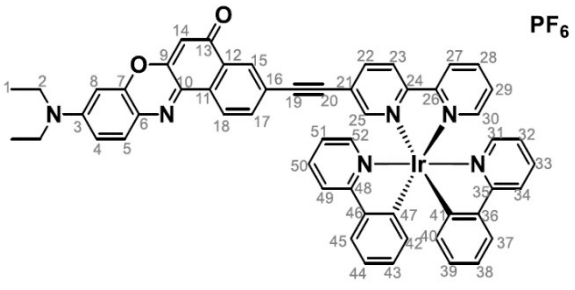

HRMS (m/z, MALDI-TOF, MeOH) $[M\text{-}PF_6]^+$ $(C_{54}H_{40}N_6O_2Ir)+$, Calculated mass: 997.2842; Found: 997.2830.

UV visible absorption (MeCN): λ_{abs} (Ɛ) 340 nm (28,300 $M^{-1}cm^{-1}$); 560 nm (34,900 $M^{-1}cm^{-1}$).

Emission (MeCN): λ_{em} 635 nm (λ_{ex} 340/ 560 nm).

[Ir(2-phenylpyridine)$_2$(5-(2ENR)-2, 2'-bipyridine)]PF_6; **[Ir-2ENR]PF_6**

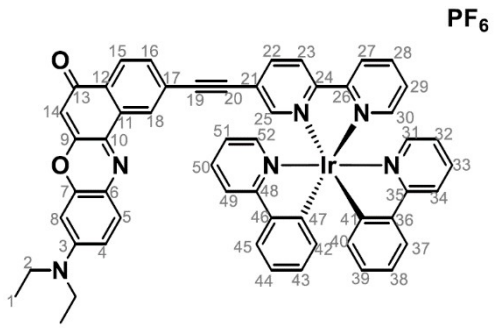

Ir1 (0.05 g, 0.06 mmol), **2ENR** (0.05 g, 0.15 mmol) and $Pd(PPh_3)_4$ (0.007 g, 0.006 mmol) were dissolved in MeCN (2.5 mL) and Et_3N and the reaction mixture was heated to 80 ˚C for 24 h under Ar. The solvent was evaporated *in vacuo* and the crude product purified *via* column chromatography (silica, CH_2Cl_2, MeOH 99:1 v/v) followed by treatment with KPF_6 to yield **Ir-2ENR** as a dark purple solid (0.020 g, 30 %).

δH (Acetone-d_6, 600 MHz, 25 ˚C): 8.95 (d, $^3J_{HH}$ 8.4 Hz, 1H, H-23), 8.92 (d, $^3J_{HH}$ 8.1 Hz, 1H, H-27), 8.67 (d, $^3J_{HH}$ 1.5 Hz, 1H, H-18), 8.52 (dd, $^3J_{HH}$ 8.4 Hz, $^4J_{HH}$ 1.9 Hz, 1H, H- 22), 8.34 (t, $^3J_{HH}$ 7.7 Hz, 1H, H-28), 8.28-8.26 (m, 3H, H-34, H-49, H-25), 8.21 (d, $^3J_{HH}$ 8.1 Hz, 1H, H-15), 8.14 (d, $^3J_{HH}$ 4.4 Hz, 1H, H-30), 8.05 (d, $^3J_{HH}$ 5.8 Hz, 1H H-52), 8.02- 7.97 (m, 2H, H-33, H-50), 7.94 (d, $^3J_{HH}$ 7.8 Hz, 1H, H-37), 7.92 (d, $^3J_{HH}$ 7.0 Hz, 1H, H- 45), 7.87 (d, $^3J_{HH}$ 5.2 Hz, 1H, H-31), 7.75 (t, $^3J_{HH}$ 6,4 Hz, 1H, H-29), 7.72 (dd, $^3J_{HH}$ 8.1 Hz, $^3J_{HH}$ 1.6 Hz, 1H, H-16), 7.65 (d, $^3J_{HH}$ 9.1 Hz, 1H, H-5), 7.20-7.18 (m, 2H, H-32, H-51), 7.10 (t, $^3J_{HH}$ 7.8 Hz, 1H, H-38), 7.06 (t, $^3J_{HH}$ 7.7 Hz, 1H, H-44), 6.98 (t, $^3J_{HH}$ 7.4 Hz, 1H, H-39), 6.95-6.91 (m, 2H, H-43, H-4), 6.69 (d, $^4J_{HH}$ 2.7 Hz, 1H, H-8), 6.41 (d, $^3J_{HH}$ *6.8 Hz, 1H, H-40), 6.35 (d,* $^3J_{HH}$ *7.6 Hz, 1H, H-42), 7.27 (s, 1H, H-14), 3.63 (q,* $^3J_{HH}$ *7.1 Hz, 4H, H-2), 1.28 (t,* $^3J_{HH}$ *7.2 Hz, 6H, H-1) ppm.*

δC (Acetone-d_6, 151 MHz, 25 ˚C): 182.00 (CQ, C-13), 168.66 (CQ, C-35), 168.52 (CQ, C- 48), 156.34 (CQ, C-26), 156.29 (CQ, C-24), 153.37 (CH, C-25), 153.34 (CQ, C-9), 152.55 (CQ, C-3), 151.75 (CH, C-30), 150.89 (CQ, C-41), 150.67 (CQ, C-47), 150.58 (CH, C-52), 150.23 (CH, C-31), 147.98 (CQ, C-7), 145.04 (CQ, C-36), 144.92 (CQ, C-46), 142.64 (CH, C-22), 140.54 (CH, C-28), 139.70 (CH, C-33), 139.64 (CH, C-50), 138.77 (CQ, C-10), 133.31 (CQ, C-11), 132.90 (CH, C-16), 132.68 (CQ, C-12), 132.63 (CH, C-40)132.43 (CH, C-42), 132.14 (CH, C-5), 131.44 (CH, C-39), 131.33 (CH, C-43), 129.78 (CH, C- 29), 127.84 (CH, C-18), 126.82 (CH, C-15), 126.30 (CH, C-27), 126.02 (CH, C-37), 125.87 (CH, C-45), 125.67 (CQ, C-6), 125.52 (CH, C-23)), 125.08 (CQ, C-21), 124.83 (CQ, C-17), 124.57 (CH, 2C, C-32, C-51), 123.62 (CH, C-38), 123.54 (CH, C-44), 121.01 (CH, C-34), 120.84 (CH, C-49), 111.35 (CH, C-4), 106.08 (CH, C-14), 97.14 (CH, C-8), 96.59 (CQ, C-19), 86.99 (CQ, C-20), 45.73 (CH2, 2C, C-2), 12.84 (CH3, 2C, C-1) ppm.

δF (Acetone-d_6, 376 MHz, 25 ˚C): -72.64 (d, 1JFP 707.4 Hz) ppm.

HRMS (m/z, ESI$^+$, MeOH) [M-PF6]$^+$ $(C_{54}H_{40}N_6O_2Ir)^+$, Calculated mass: 997.2840; Found: 997.2838.

UV visible absorption (MeCN): λ_{abs} (Ɛ) 340 nm (27,800 M^{-1} cm^{-1}); 550 nm (17,900 M^{-1} cm^{-1}).

Emission (MeCN): λ_{em} 630 nm (λ_{ex} 340/ 550 nm).

[Ir(2-phenylpyridine)$_2$(5-(2ENR)-2, 2'-bipyridine)]Cl; **[Ir-2ENR]Cl**

[Ir-2ENR]PF$_6$ (0.02 g, 0.018 mmol) was deposited on a silica column and eluted with MeCN, H_2O, KCl(aq) (90:10:1 v/v/v). The solvent was evaporated *in vacuo* to yield **[Ir-2ENR]Cl** as a purple solid (0.015 g, 80 %).

δF (CD_3OD, 376 MHz, 25 ˚C): no signal
δCl (CD_3OD, 39 MHz, 25 ˚C): -31.07 ppm

[Ir(2-phenylpyridine)$_2$(5-(3ENR)-2, 2'-bipyridine)]Cl; **[Ir-3ENR]Cl**

[Ir-3ENR]PF$_6$ (0.023 g, 0.020 mmol) was deposited on a silica column and eluted with MeCN, H_2O, KCl(aq) (90:10:1 v/v/v). The solvent was evaporated *in vacuo* to yield **[Ir-3ENR]Cl**as a purple solid (0.020 g, 95 %).

δF (CD_3OD, 376 MHz, 25 ˚C): no signal
δCl (CD_3OD, 39 MHz, 25 ˚C): -32.68 ppm

Spectral Characterisation

HRMS

Table S1. HRMS analysis of **3ENR-bpy** and **[Ir-2ENR]$^+$ and [Ir-3ENR]$^+$**.

Compound	Chemical Formula	Molecular Ion	Calculated Mass	Found Mass	Ionisation source
3ENR-bpy	$C_{32}H_{25}N_4O_2$	$[M-H]^+$	497.1972	497.1973	ESI
[Ir-ENR]PF$_6$,	$C_{54}H_{40}N_6O_2Ir$	$[M-PF_6]^+$	997.2842	997.2830	MALDI
[Ir-ENR]PF$_6$,	$C_{54}H_{40}N_6O_2Ir$	$[M-PF_6]^+$	997.2842	997.2838	MALDI

NMR Spectroscopy

3ENR-bpy

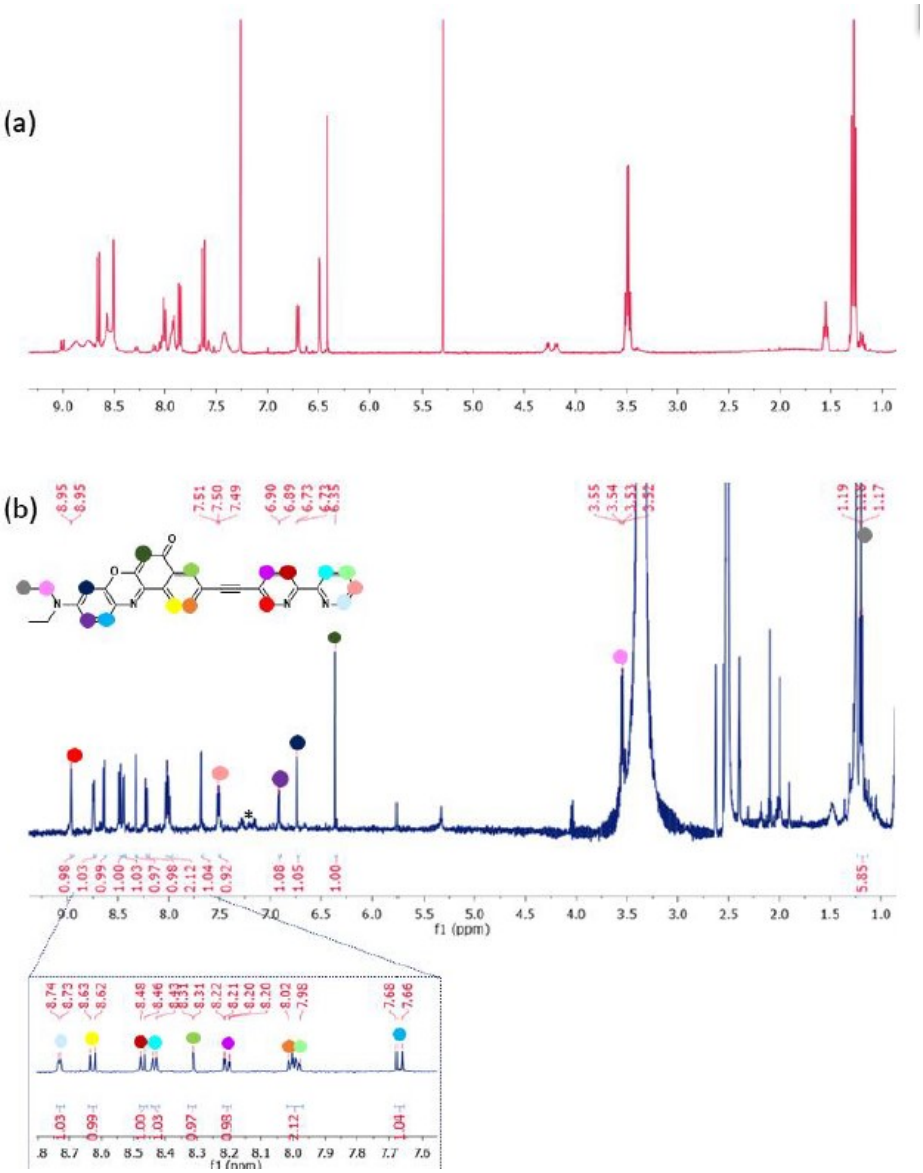

Fig. S1. ^{1}H NMR spectra of **3ENR-bpy** recorded in (a) $CDCl_3$ (400 MHz, 298 K); (b) D_6-DMSO (600 MHz, 298 K). * denotes residual toluene solvent.

[Ir-2ENR]PF_6

In **[Ir-2ENR]PF_6**, the signal associated with the proton adjacent to the cyclometalating carbon appeared upfield, which is typical in Ir(III) cyclometalated species.[1] The fully assigned ^{1}H and $^{13}C\{^{1}H\}$ NMR spectra are presented in Fig. S2 and 3 , respectively.

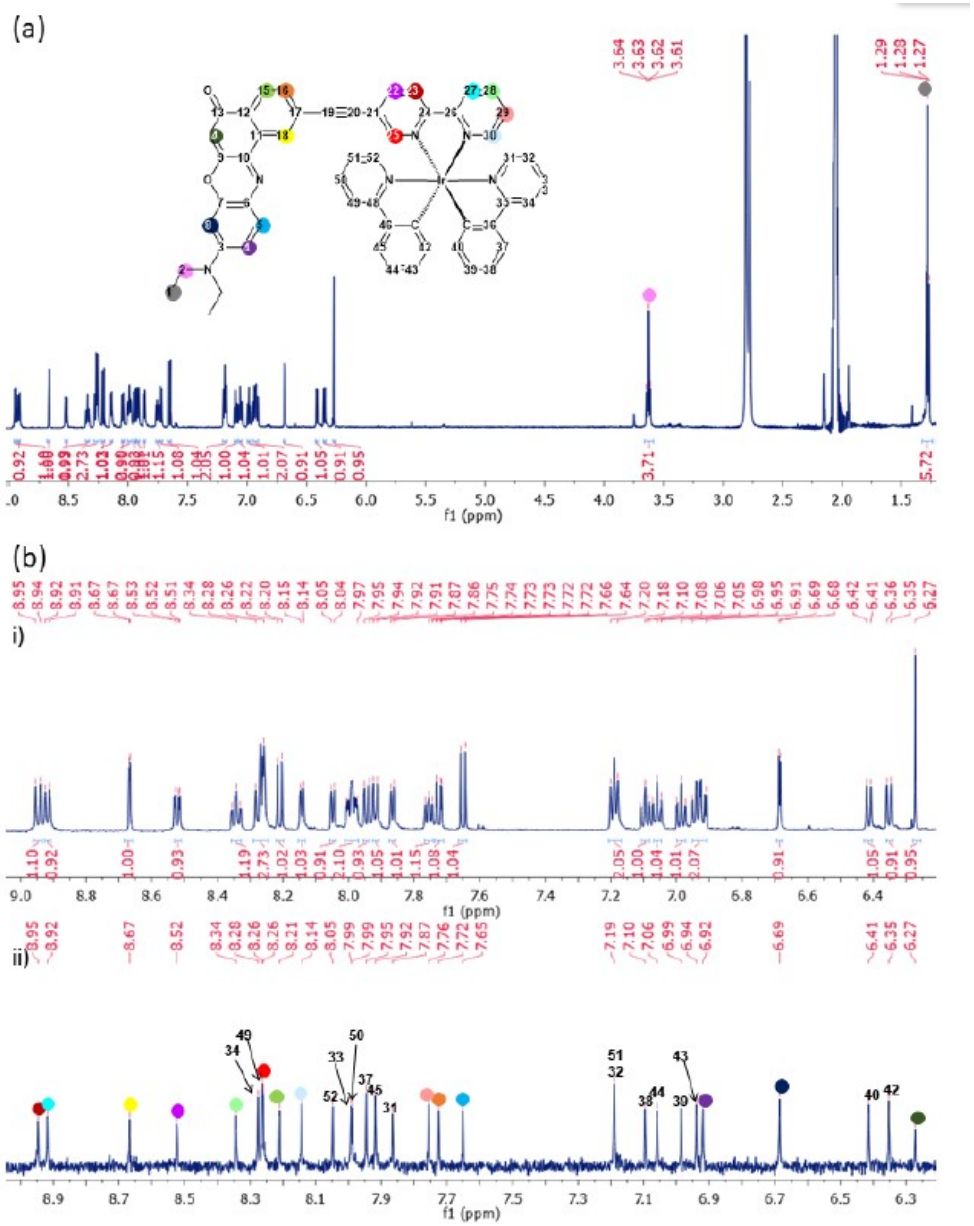

Fig. S2. Assigned 1H NMR spectrum of **[Ir-2ENR]PF_6** (acetone-D_6, 600 MHz, 298 K) (a) full spectrum; (b) expansion of δ 9.00 – 6.25 ppm region (i) ^{1}H NMR spectrum, and (ii) PSYCHE spectrum.

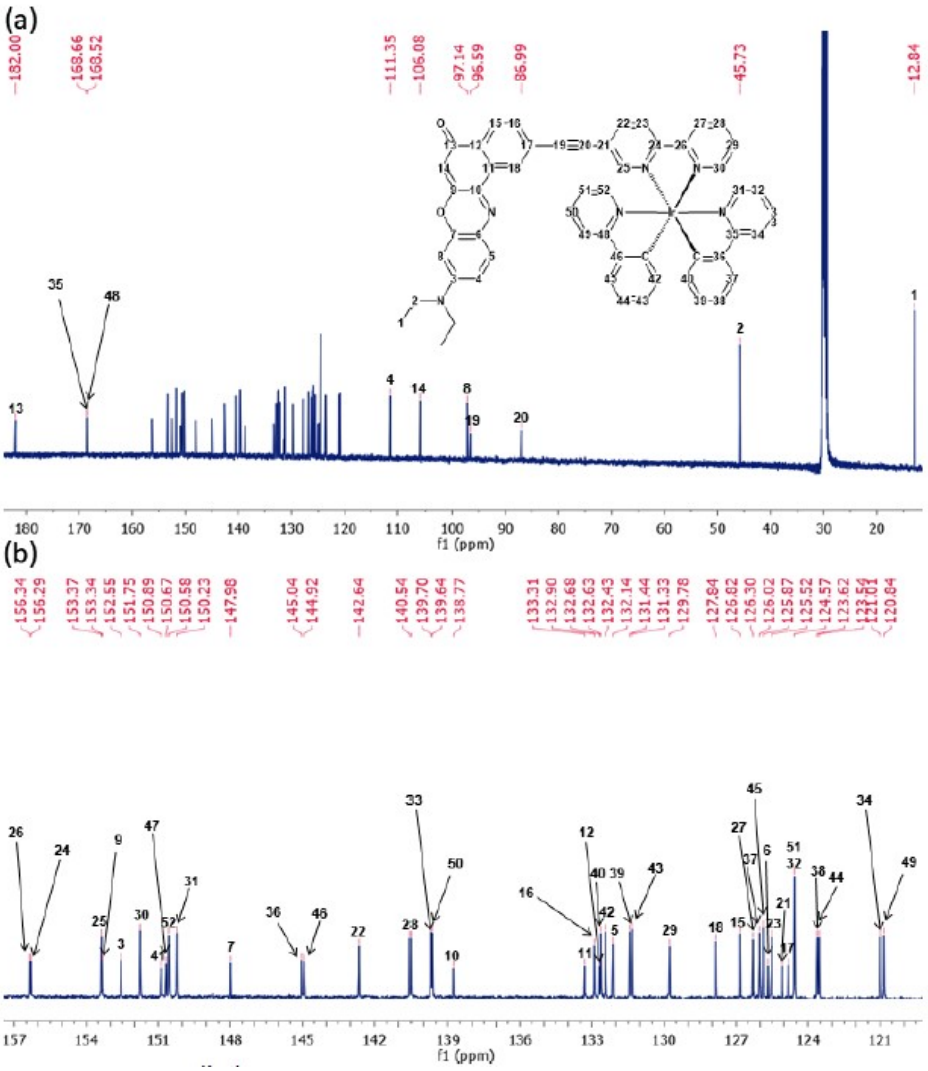

Fig. S3. Assigned $^{13}C\{^{1}H\}$ spectrum of **[Ir-2ENR]PF$_6$** (acetone-D$_6$, 150 MHz, 298 K) (a) full spectrum; (b) expansion of δ 160– 120 ppm region.

[Ir-3ENR]PF$_6$

In **[Ir-3ENR]PF$_6$**, the signal for the proton at position 25 appears at approximately δ 8.09 ppm. This is more downfield than in the analogous Ru(II) complex, **[Ru-3ENR](PF$_6$)$_2$** (cf. δ 7.95 ppm). Despite the **3ENR-bpy** ligand being coordinated to the more positively charged Ir(III) metal centre, the presence of the ppy ancillary ligands, each containing an anionic carbon atom, resulted in the coordinating nitrogen atom donating less electron density and therefore this nitrogen is more deshielding than in the **[Ru-2ENR](PF$_6$)$_2$** and the resonance for the proton adjacent to the coordinating nitrogen appeared more downfield than in **[Ru-3ENR](PF$_6$)$_2$** . The fully assigned ^{1}H and $^{13}C\{^{1}H\}$ NMR spectra for **[Ir-3ENR]PF$_6$** are presented in Fig. S4 and 5, respectively.

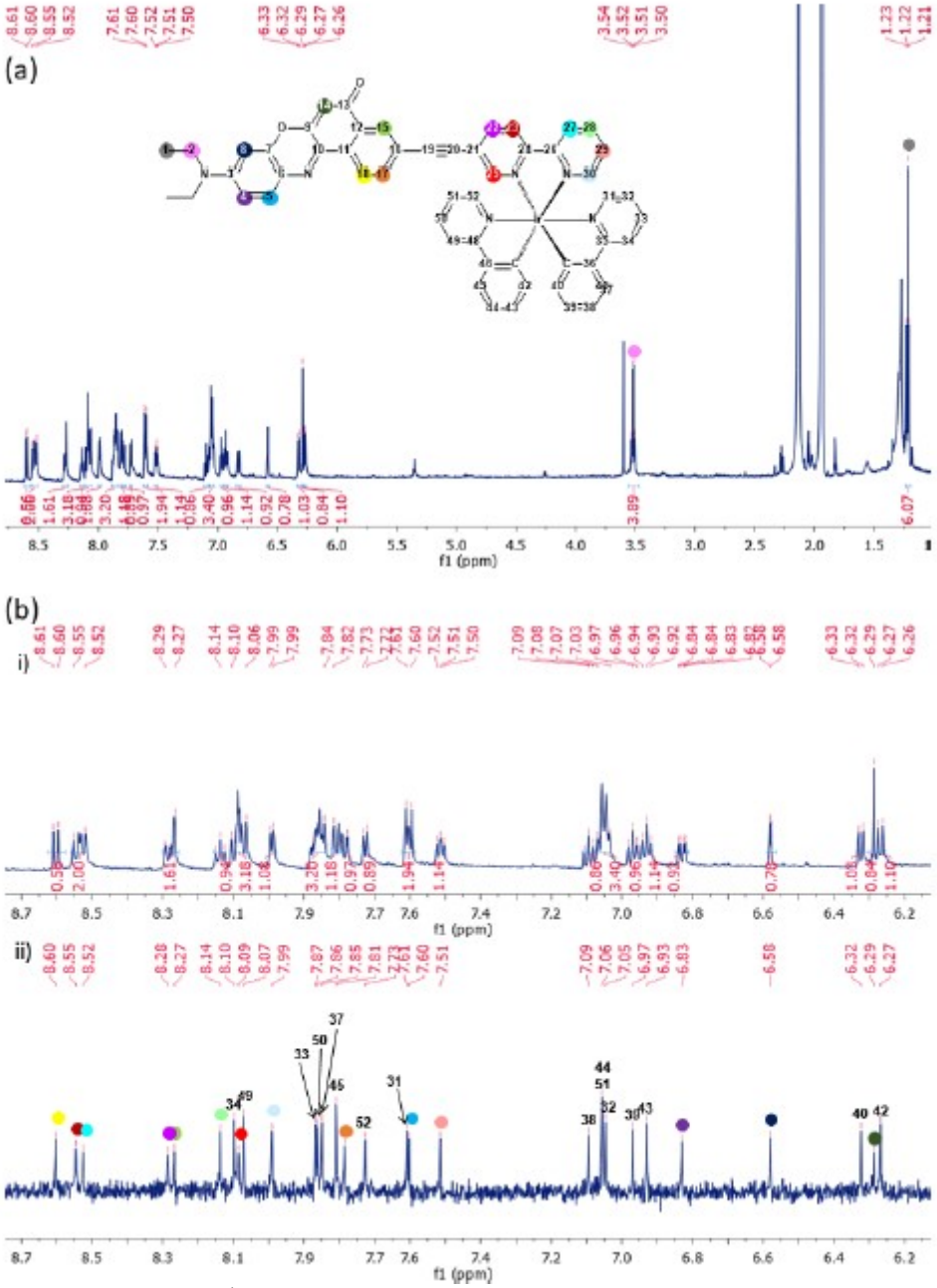

Fig. S4. Assigned ^{1}H NMR spectrum of **[Ir-3ENR]PF$_6$** (CD_3CN, 600 MHz, 298 K) (a) full spectrum; (b) expansion of δ 9.00 – 6.25 ppm region (i) 1H NMR spectrum, and (ii) PSYCHE spectrum.

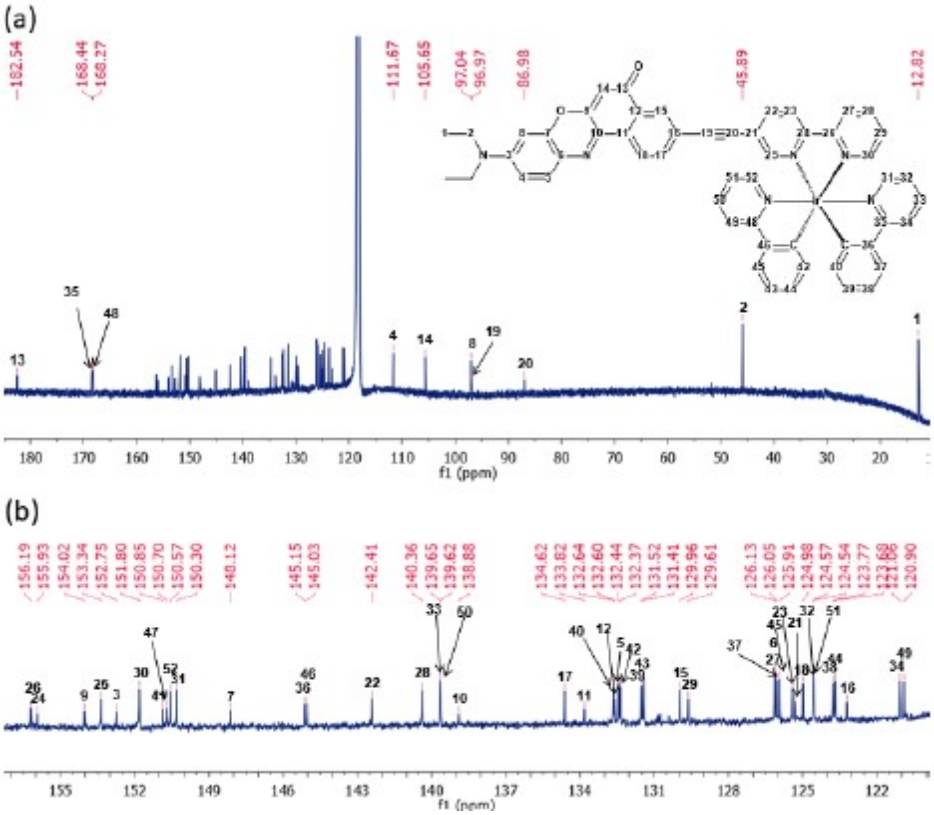

Fig. S5. Assigned $^{13}C\{^{1}H\}$ spectrum of **[Ir-3ENR]PF_6** (CD_3CN, 150 MHz, 298 K) (a) full spectrum; (b) expansion of δ 160– 120 ppm region.

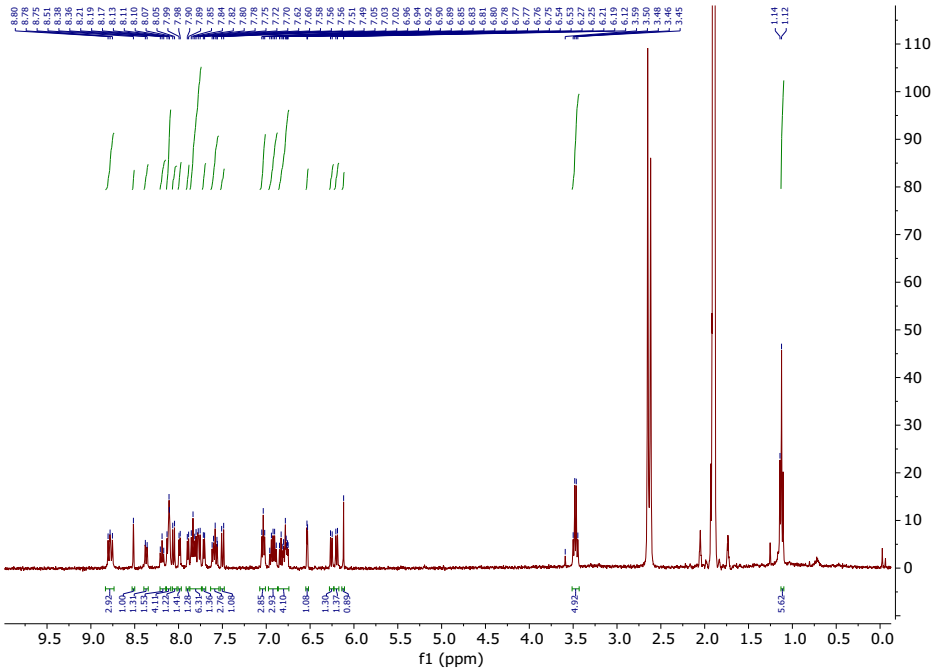

[Ir-2ENR]Cl

Fig. S6. ^{1}H NMR of **[Ir-2ENR]Cl** (400 MHz, Acetone, 298 K).

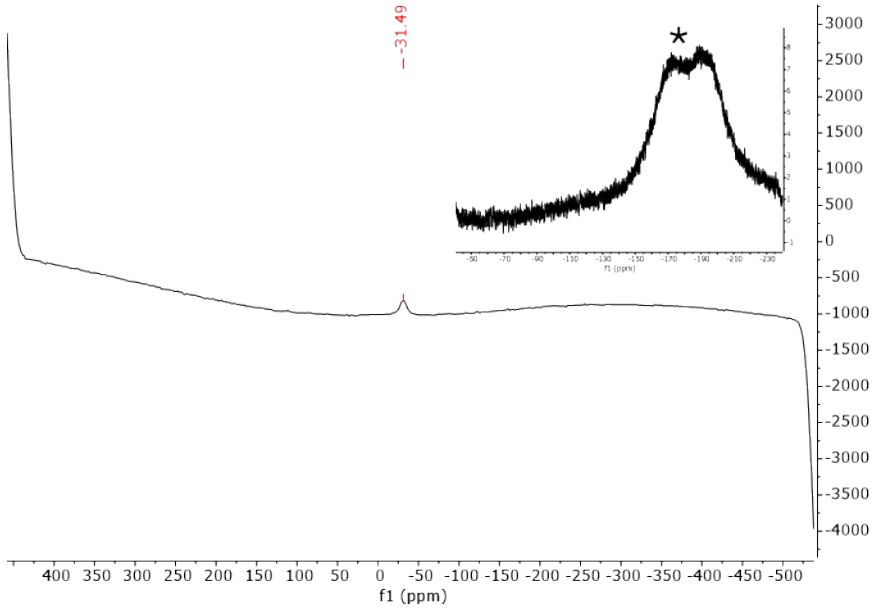

Fig. S7. ^{35}Cl NMR of **[Ir-2ENR]Cl** (CD_3OD, 39 MHz, 298 K); inset: ^{19}F NMR of **[Ir-2ENR]Cl** (CD_3OD, 376 MHz, 298 K); asterisk denotes signal from NMR tube glass.

[Ir-3ENR]Cl

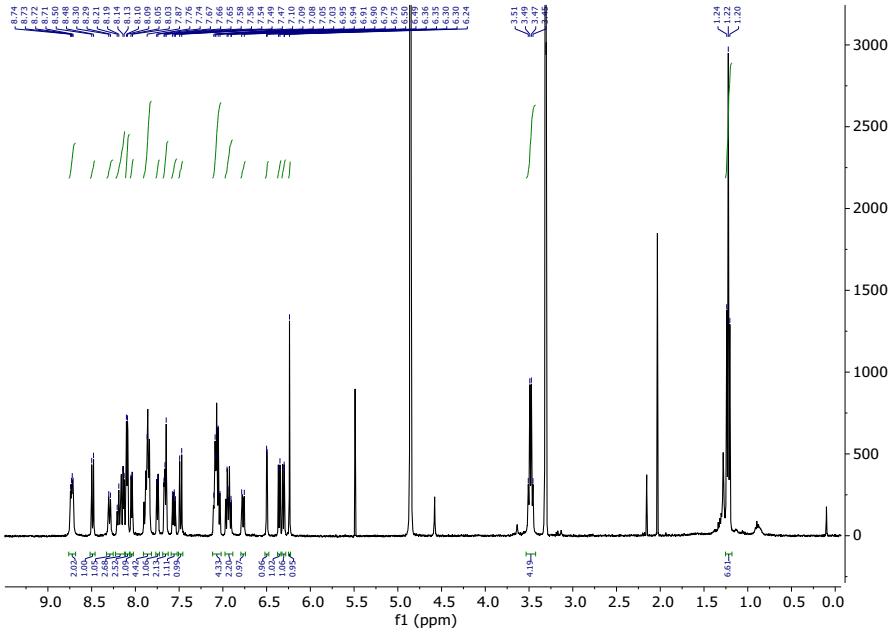

Fig. S8. ^{1}H NMR of **[Ir-3ENR]Cl** (400 MHz, MeOD, 298 K).

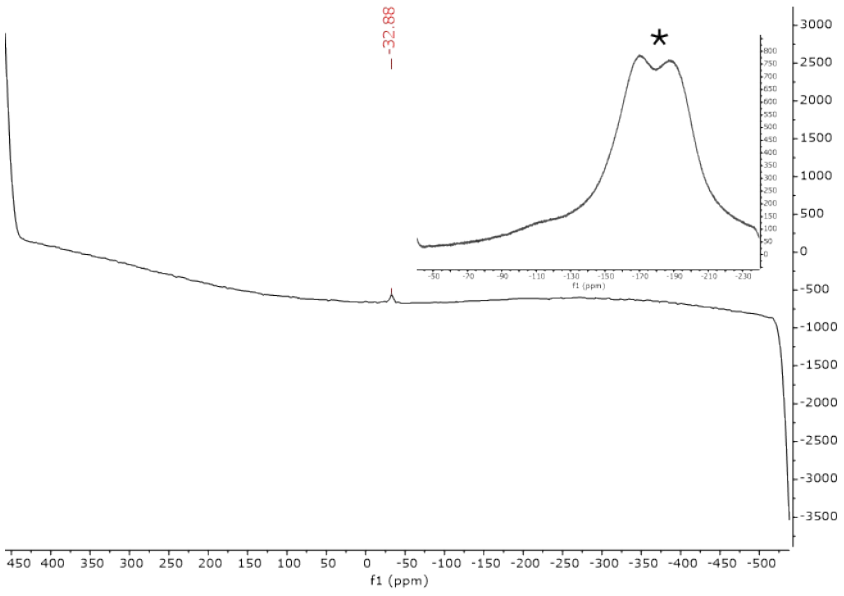

Fig. S9. ^{35}Cl NMR of **[Ir-3ENR]Cl** (CD_3OD, 39 MHz, 298 K); inset: ^{19}F NMR of **[Ir-3ENR]Cl** (CD_3OD, 376 MHz, 298 K); asterisk denotes signal from NMR tube glass.

Electrochemistry

Cyclic and differential pulse voltammetry (CV and DPV) were employed to investigate the electrochemical properties of **Ir[3ENR]PF_6**. CV measurements were performed at scan rates of 40 and 100 mV s^{-1} under N_2 or air, in the dark or under light, and at 0–5 °C. The voltammograms were similar across conditions, and the redox processes were quasi-reversible (**Figure S10-11**).

A quasi-reversible oxidation at 1.25–1.31 V vs SCE is assigned to the Ir^{3+}/Ir^{4+} couple, consistent with the 1.27 V value reported for $[Ir(ppy)_2(bpy)]^+$.[2-4] This indicates that incorporation of the **3ENR** chromophore has minimal effect on the metal-centred oxidation. This oxidation corresponds to the HOMO level of the complex and is directly related to the ^{1}MLCT absorption shoulder around 340 nm, where electron density is transferred from the Ir centre to the bpy/ppy ligands. Two additional irreversible oxidations at 0.89–1.06 V vs SCE are attributed to the NR chromophore and correlate with the NR-centred ^{1}ILCT absorption bands between 440-700 nm.

Two quasi-reversible reductions at –1.38 to –1.81 V vs SCE, assigned to bpy- and ppy-centred reductions, define the LUMO levels and underpin the energy of the MLCT and ILCT. The HOMO-LUMO gap associated with the NR-bpy ligand was estimated to be 1.508 eV based on the equations below, where E'_{red} and E'_{ox} are onset reduction and oxidation potentials versus the $Ag/AgNO_3$ reference electrode.[5] The estimated optical bandgap calculated 1.837 eV was higher (onset absorption of 670 nm), than the electrochemical.

$$E_{LUMO} = (E'_{red} + 4.4)eV$$

$$E_{HOMO} = (E'_{ox} + 4.4)eV$$

$$E_{optical} = h\nu\ (eV) = \frac{1239.8(eV\ x\ nm)}{\lambda\ (nm)}$$

Under O_2 or light exposure, the CVs shift to more positive potentials, and the reductions become partially irreversible at lower scan rates. This may reflect some interaction with oxygen and the formation of long-lived ^{3}ILCT states as observed in nanosecond time-resolved spectroscopy. DPV measurements (**Figure S12**) corroborate the assignments, providing better-resolved peaks that align with the redox profiles of the **Ir-1** precursor and the free **3ENR** chromophore (**Figure S11**). [2, 3, 6, 7] A summary of all measured redox potentials, referenced against both $Ag/AgNO_3$ and SCE, is presented in **Table S2**.

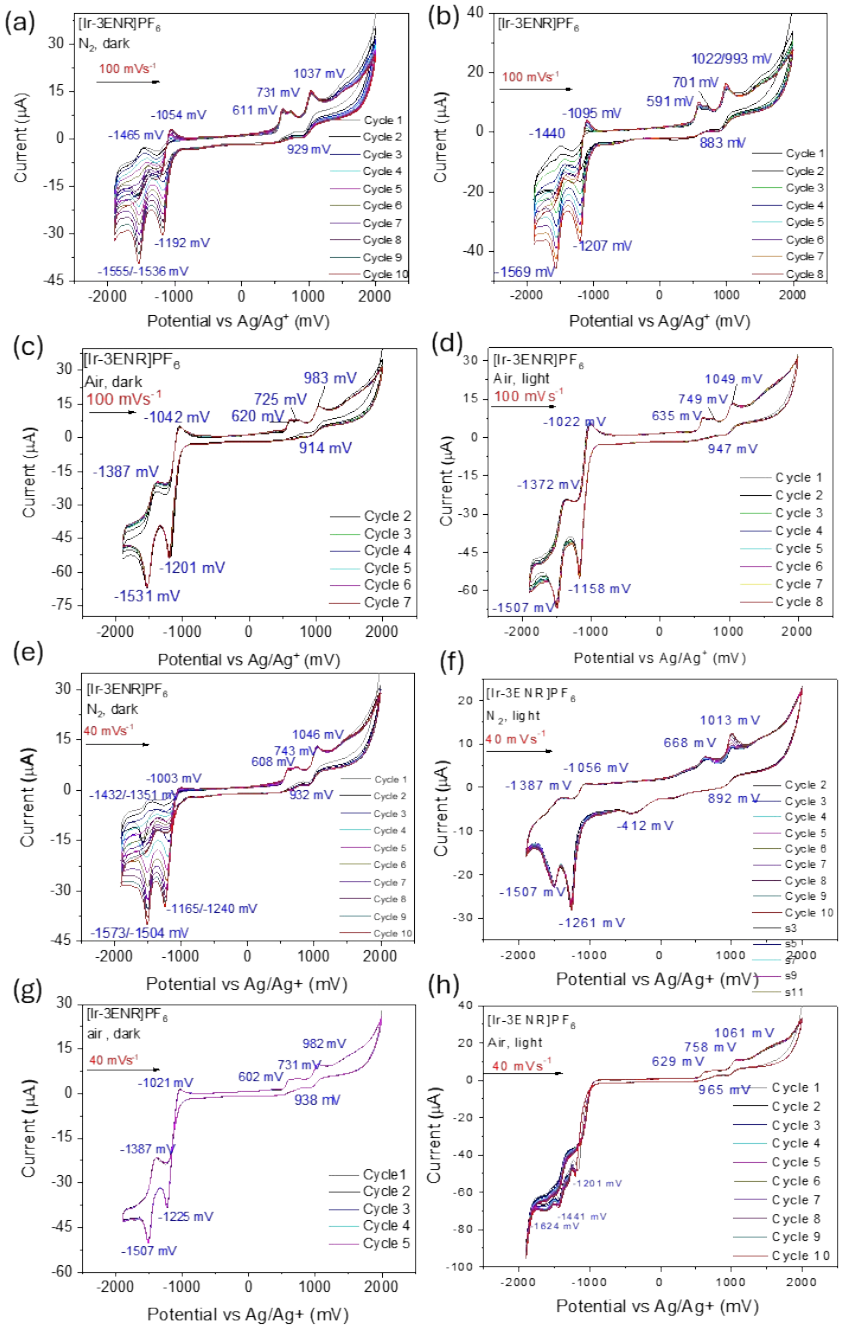

Figure S10. Cyclic voltammograms of **Ir[3-ENR]PF$_6$** (1 mM) at Pt electrode in 0.1 M TBAPF$_6$ at 100 mVs^{-1} (a) under N_2 in the dark; (b) under N_2 exposed to light; (c) under air in the dark; (d) under air and exposed to light. Cyclic voltammograms of **Ir[3-ENR]PF$_6$** (1 mM) at Pt electrode in 0.1 M TBAPF$_6$ at 40 mVs^{-1} (e) under N_2 in the dark; (f) under N_2 exposed to light; (g) under air in the dark; (h) under air and exposed to light.

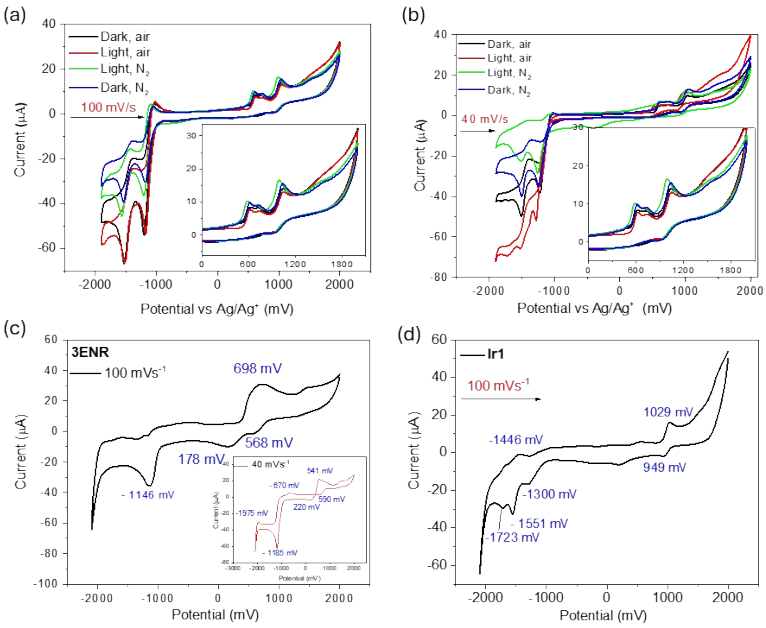

Figure 11. Cyclic voltammograms of **Ir[3-ENR]PF$_6$** (1 mM) at Pt electrode in 0.1 M TBAPF$_6$ (a) at 100 mVs^{-1} and (b) at 40 mVs^{-1} under N_2 in the dark (black), under N_2 exposed to light (green), under air in the dark (blue) and under air and exposed to light (red). Cyclic voltammograms of (c) **3-ENR** (1 mM) and **Ir-1** (1 mM) at Pt electrode in 0.1 M TBAPF$_6$ at 100 mVs^{-1}.

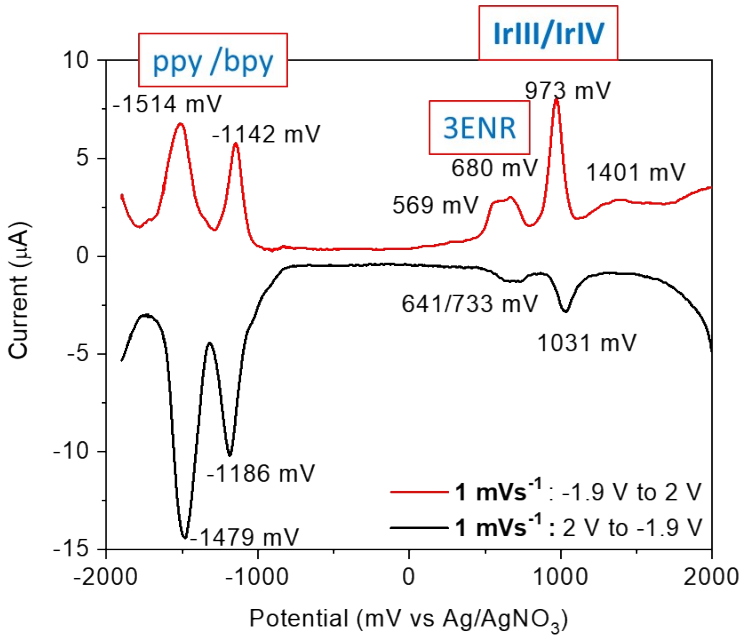

Figure S12. Differential pulse voltammograms of **Ir[3-ENR]PF$_6$** (1 mM) at Pt electrode in 0.1 M TBAPF$_6$ at 1 mVs^{-1} under N_2 in the dark 2.0 V to -1.9 V (black) and -1.9 V to 2.0 V (red).

Table S2. Oxidation and reduction potentials, $E_{1/2}$ and ΔE_p values (mV) referenced to $Ag/AgNO_3$ and SCE[8] at scan rates of 40 mV/s and 100 mV/s and solutions of **Ir[3-ENR]PF_6** exposed or protected from light and under air or N_2.

		Ox vs Ag/Ag+ (mV)	Ox vs SCE (mV)	Red vs Ag/Ag+ (mV)	Red vs SCE (mV)	$E_{1/2}$ vs Ag/Ag+ (mV)	ΔE_p (mV)	$E_{1/2}$ vs SCE (mV)
	100 mVs^{-1}							
Dark, N_2	Ir III/IV	1037	1335	929	1227	**983**	108	**1281**
	1	731	1029	-	-			
	2	611	909	-	-			
	3	-1054	-1352	-1192	-1490	**-1123**	138	**-1421**
	4	-1465	-1763	-1555	-1853	**-1510**	90	**-1808**
Light, N_2	Ir III/IV	1022	1320	883	1181	**953**	121	**1251**
	1	701	999	-	-	-	-	-
	2	591	889	-	-	-	-	-
	3	-1095	-1393	-1207	-1505	**-1151**	112	**-1449**
	4	-1440	-1738	-1569	-1867	**-1505**	129	**-1803**
Dark, air	Ir III/IV	983	1281	914	1212	**952**	69	**1250**
	1	725	1023	-	-	-	-	
	2	620	918	-	-	-	-	
	3	-1042	-1340	-1201	-1499	**-1122**	159	**-1420**
	4	-1387	-1785	-1531	-1829	**-1459**	144	**-1757**
Light, air	Ir III/IV	1049	1347	947	1245	**998**	102	**1296**
	1	749	1047	-	-	-	-	-
	2	635	933	-	-	-	-	-
	3	-1022	-1320	-1158	-1456	**-1090**	136	**-1388**
	4	-1372	-1670	-1507	-1805	**-1440**	135	**-1738**
	40 mVs^{-1}							
Dark, N_2	Ir III/IV	1046	1344	932	1230	**989**	114	**1287**
	1	743	1041	-	-	-	-	-
	2	608	906	-	-	-	-	-
	3	-1003	-1301	-1165	-1463	**-1084**	162	**-1382**
	4	-1432	-1730	-1543	-1841	**-1488**	111	**-1786**
Light, N_2	Ir III/IV	1013	1311	892	990	**953**	121	**1251**
	1	-	-	-	-	-	-	-
	2	668	966	-	-	-	-	-
	3	-1056	-1354	-1261	-1559	**1159**	205	**-1456**
	4	-1387	-1685	-1507	-1805	**-1447**	120	**-1745**
Dark, air	Ir III/IV	982	1280	938	1236	**960**	44	**1258**
	1	731	1029	-	-	-	-	
	2	602	900	-	-	-	-	
	3	-1021	-1319	-1225	-1523	**-1123**	204	**-1421**
	4	-1387	-1685	-1507	-1805	**-1447**	120	**-1745**
Light, air	Ir III/IV	1061	1359	965	1263	**1013**	96	**1311**
	1	758	1056	-	-	-	-	-
	2	629	927	-	-	-	-	-
	3	-	-	-1201	-1499	-	-	-
	4	-	-	-1441	-1739	-	-	-
	5	-	-	-1624	-1922	-	-	-

Photophysical Studies

3ENR-bpy

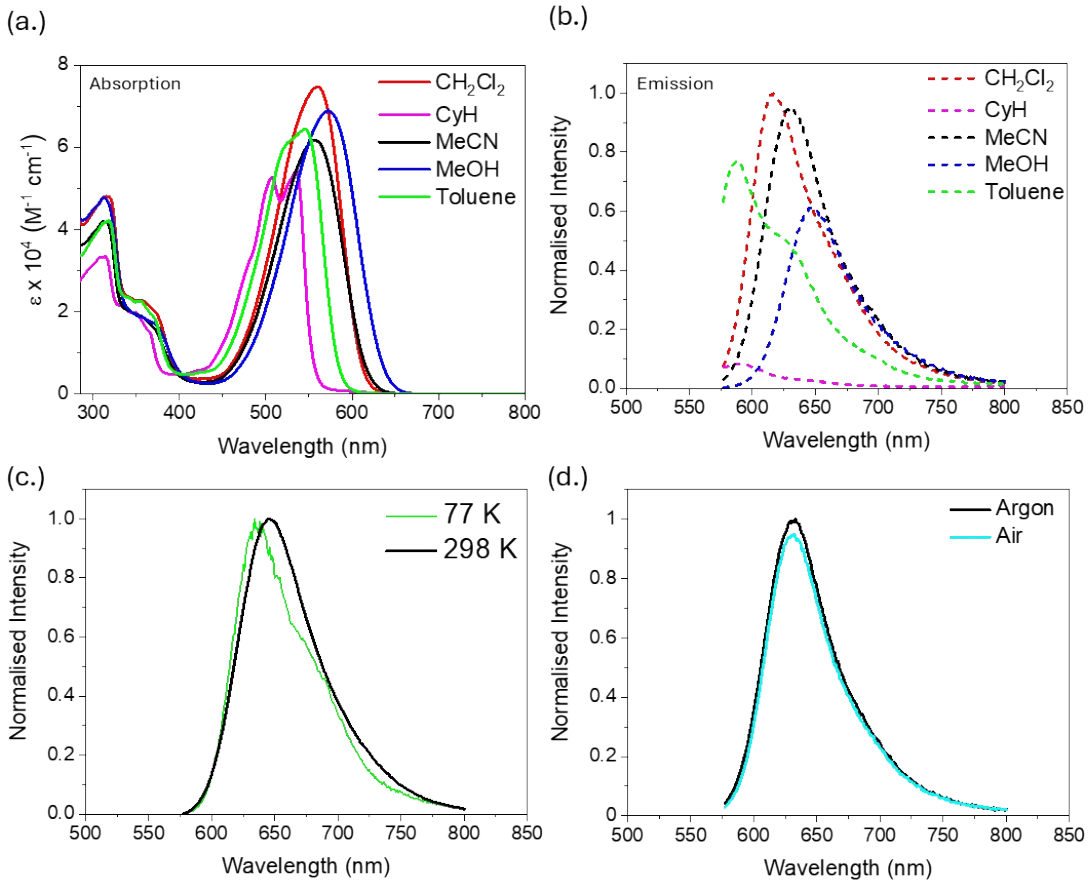

Fig. S13. Solvatochromism studies (a) UV-visible absorption and (b) emission of **3ENR-bpy** in CyH (cyclohexane), Toluene, DCM (dichloromethane), MeCN (acetonitrile), MeOH (methanol), and toluene; [1 x 10^{-5} M], 298 K. (c) Normalised emission of **3ENR-bpy** in at 77 and 298 K in EtOH/MeOH (4:1, v/v). (d) Normalised emission of **3ENR-bpy** in acetonitrile under air and inert atmosphere; [1 x 10^{-5} M], 298 K.

Table S3. UV-visible and emission data for **3ENR-bpy**, and cyclohexane, toluene, DCM, methanol and acetonitrile. [10^{-5} M], 298 K.

Solvent	λ_{abs} (nm)	ε /10^4 ($M^{-1}cm^{-1}$)	λ_{em} (nm)
CyH	506, 534	5.30, 5.36	587
Toluene	546	6.42	587
DCM	561	7.47	616
MeOH	573	6.87	647
MeCN	557	6.19	630

[Ir-2ENR]$^+$ and [Ir-3ENR]$^+$

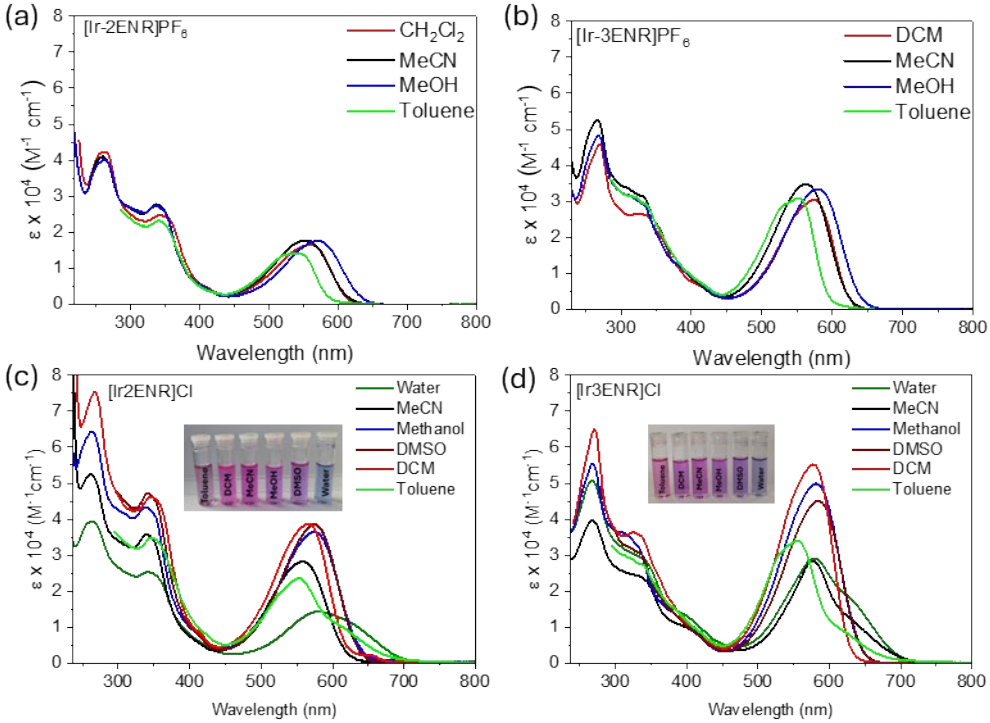

Fig. S14. UV-Visible absorption solvatochromism studies of (a,b) **[Ir-2ENR]PF$_6$**, and **[Ir-3ENR]PF$_6$** in CH_2Cl_2, MeCN, MeOH and toluene; 298 K, and (c,d) **[Ir-2ENR]Cl**, and **[Ir-3ENR]Cl** in CH_2Cl_2, MeCN, MeOH, DMSO, water and toluene; 298 K.

Table S4. UV-visible spectral data for compounds **[Ir-2ENR]Cl/PF$_6$**, **[Ir-3ENR]Cl/PF$_6$**, toluene, DCM, MeOH and MeCN [10^{-5} M], 298 K.

[Ir-2ENR]PF$_6$		[Ir-3ENR]PF$_6$		[Ir-2ENR]Cl		[Ir-3ENR]Cl	
λ_{abs} (nm)	ε /10^4 (M^{-1}cm^{-1})	λ_{abs} (nm)	ε /10^4 (M^{-1}cm^{-1})	λ_{abs} (nm)	ε /10^4 (M^{-1}cm^{-1})	λ_{abs} (nm)	ε /10^4 (M^{-1}cm^{-1})
542	1.41	553	3.10	553	2.37	553	3.39
560	1.65	575	3.05	567	3.89	578	5.52
553	1.78	562	3.48	558	2.83	578	2.82
571	1.77	580	3.35	576	3.66	581	4.98

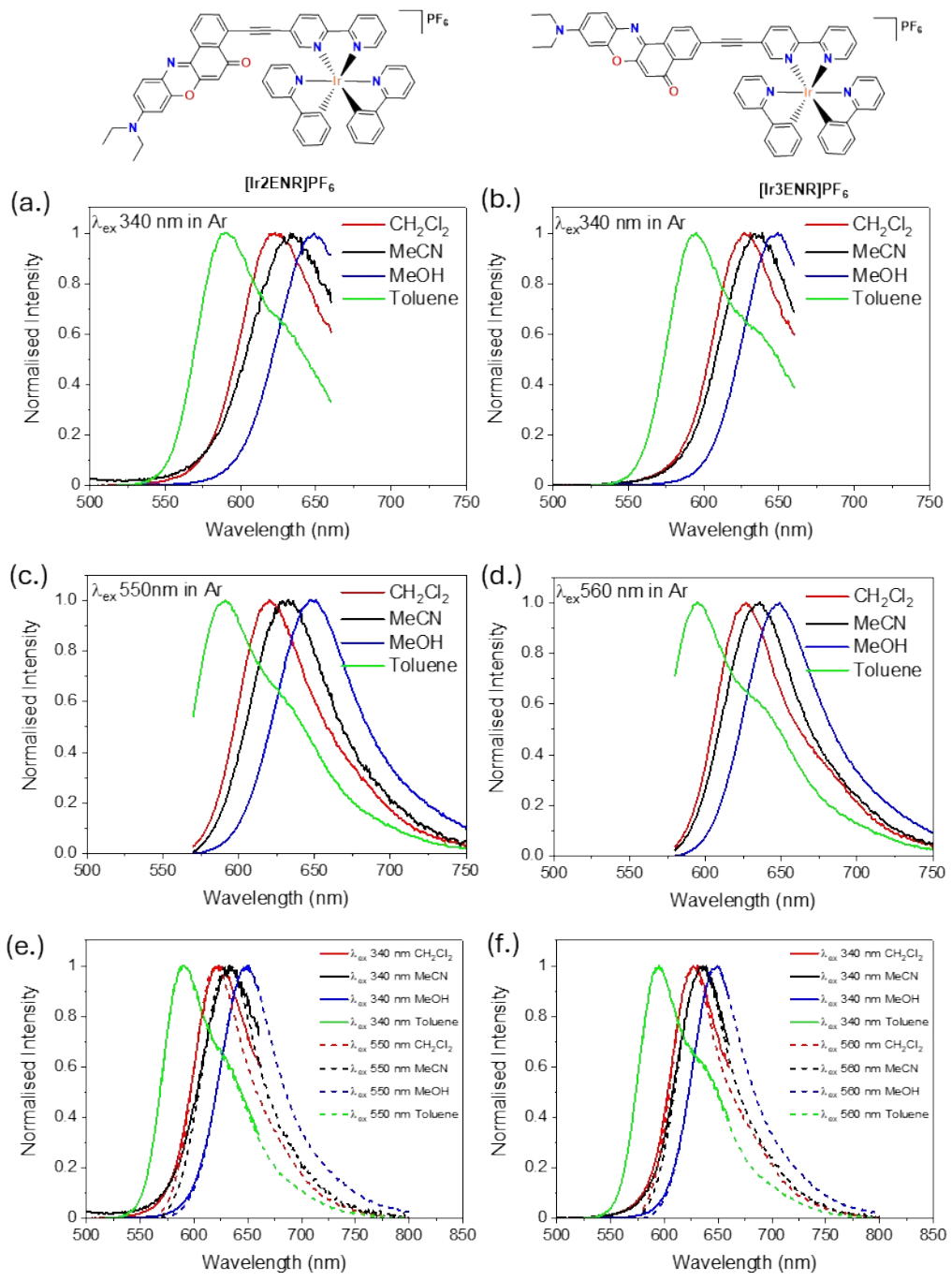

Fig. S15. Emission solvatochromism of (a,c) **[Ir-2ENR]PF_6** excited at 340 and 550 nm, and (b,d) **[Ir-3ENR]PF_6** excited at 340 and 560 nm in CH_2Cl_2, MeCN, MeOH and toluene; [1 x 10^{-5} M], 298 K. Overlapped emission spectra after excitation of 340 and 550/560 nm (e) **[Ir-2ENR]PF_6**, and (f) **[Ir-3ENR]PF_6** in CH_2Cl_2, MeCN, MeOH and toluene normalised to 1 and; [1 x 10^{-5} M], 298 K.

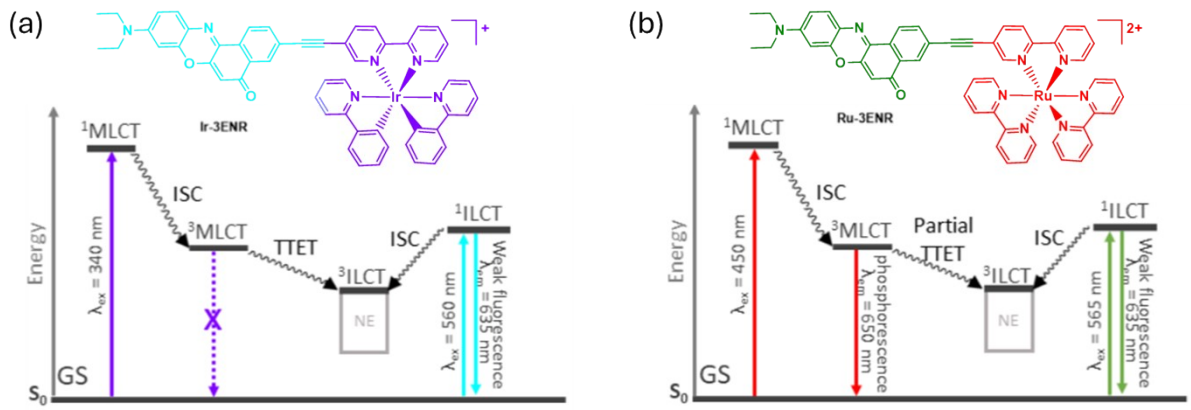

Scheme S1. Simplified Jablonski diagrams depicting the main photophysical processes in (a) (b) in deaerated solutions. Colours denote the component part of the molecules involved in the respective absorption or emissive process. As the ^{3}ILCT states are not observed directly, a box is used to indicate the unknown energy. NE = Non-Emissive.

Table S5. UV-visible and emission spectral data for compounds **[Ir-2ENR]Cl**, **[Ir-3ENR]Cl**, toluene, DCM, MeOH and MeCN [10^{-5} M], 298 K.

[Ir-2ENR]Cl	λ_{abs}[a]	ε[b]/ 10^4 (M^{-1} cm^{-1})	λ_{abs}[a]	ε[b]/ 10^4 (M^{-1} cm^{-1})	λ_{abs}[a]	ε[b]/ 10^4 (M^{-1} m^{-1})	λ_{ex}[c] (nm)	λ_{em}[d] (nm)
Toluene			348	3.48	553	2.37	546	591
DCM	267	7.52	348	4.62	567	3.89	567	619
MeCN	262	5.25	339	3.59	558	2.83	567	630
Methnaol	264	6.41	338	4.30	576	3.66	585	647
DMSO			342	4.73	574	3.86	580	644
Water	262	3.94	343	2.54	581	1.43	600	650
[Ir-3ENR]Cl								
Toluene			sh		553	3.39	552	592
DCM	270	6.48	325	3.65	578	5.52	579	626
MeCN	268	3.95	Sh		578	2.82	568	633
Methnaol	268	5.54	sh		581	4.98	587	647
DMSO			Sh	3.66	584	4.51	590	649
Water	267	5.06	sh		580	2.90	610	663

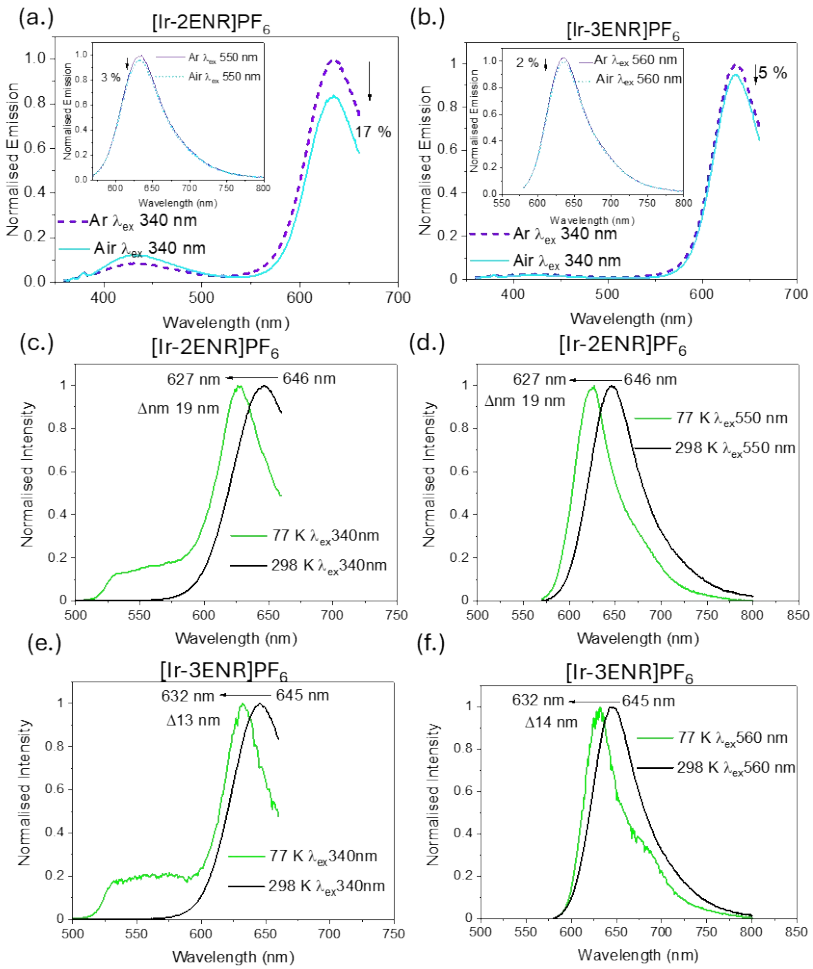

Fig. S16. Emission spectra measured under Ar (purple) and in air (blue) of (a) **[Ir-2ENR]PF$_6$** at λ_{ex} 340 nm and inset λ_{ex} 550 nm; (b) **[Ir-3ENR]PF$_6$** λ_{ex} 340 nm and inset λ_{ex} 560 nm, [10^{-5} M], 298 K. Normalised emission spectra of (c) **[Ir-2ENR][PF$_6$]** (λ_{ex} 340 nm); (d) **[Ir-2ENR][PF$_6$]** (λ_{ex} 560 nm); (e) **[Ir-3ENR][PF$_6$]** (λ_{ex} 340 nm); (f) **[Ir-3ENR][PF$_6$]** (λ_{ex} 560 nm) in EtOH/MeOH (4:1 v/v) at 77 K (green) and 298 K (black); [10^{-5} M].

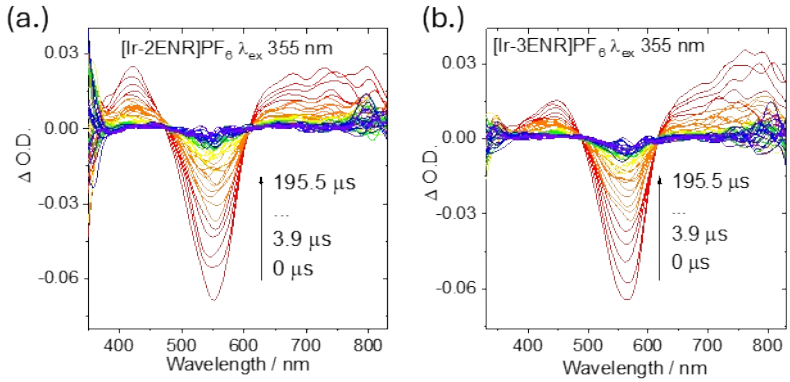

Fig. S17. Nanosecond transient absorption spectra of (a) **[Ir-2ENR]PF$_6$** and (b) **[Ir-3ENR]PF$_6$** excited with nanosecond pulsed laser at 355 nm in deaerated CH_3CN and of [10^{-5} M], 298 K.

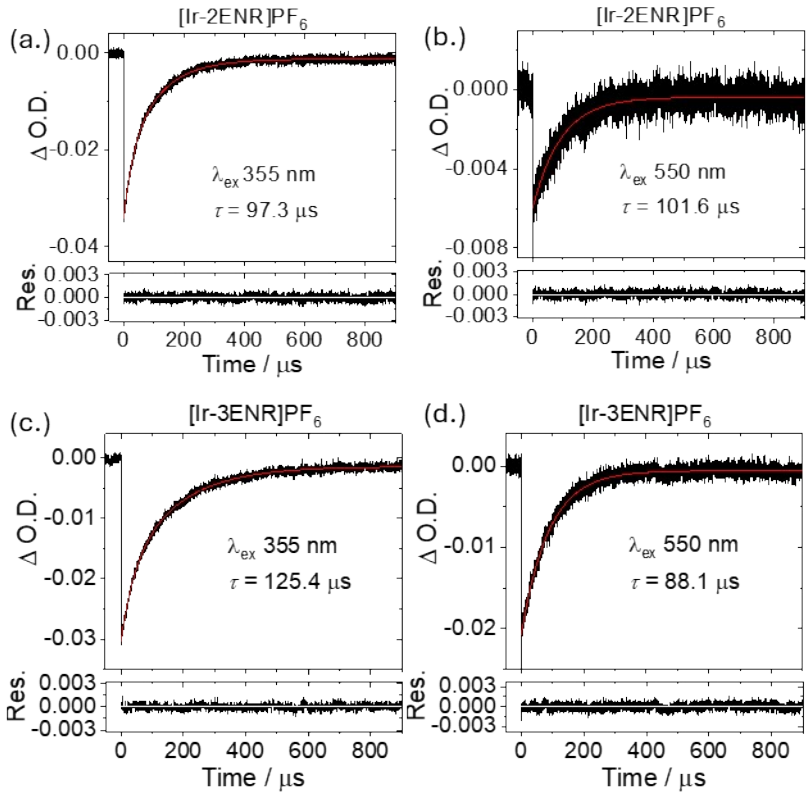

Fig. S18. Nanosecond transient absorption decay trace at 560 nm excited at 355 nm and 550 nm (a) and (b) for **[Ir-2ENR]PF$_6$** and (c) and (d) for **[Ir-3ENR]PF$_6$**. c = 1.0 × 10^{-5} M, 25 °C.

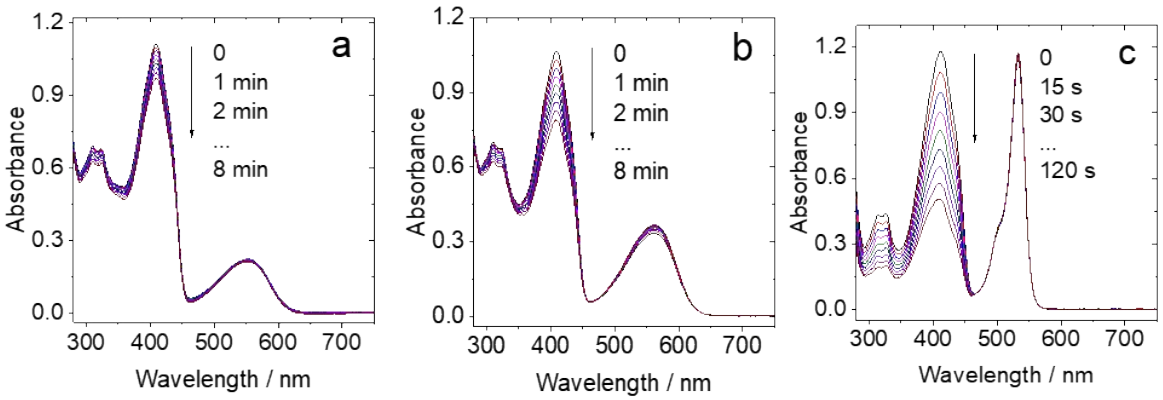

Fig. S19. The change of the UV-Vis absorption spectra with the time for the compound (a) **[Ir-2ENR]PF_6** (b) **[Ir-3ENR]PF_6** and the standard compound (c) diiodobodipy with the addition of the DPBF in CH_3CN. λ_{ex} = 550 nm.

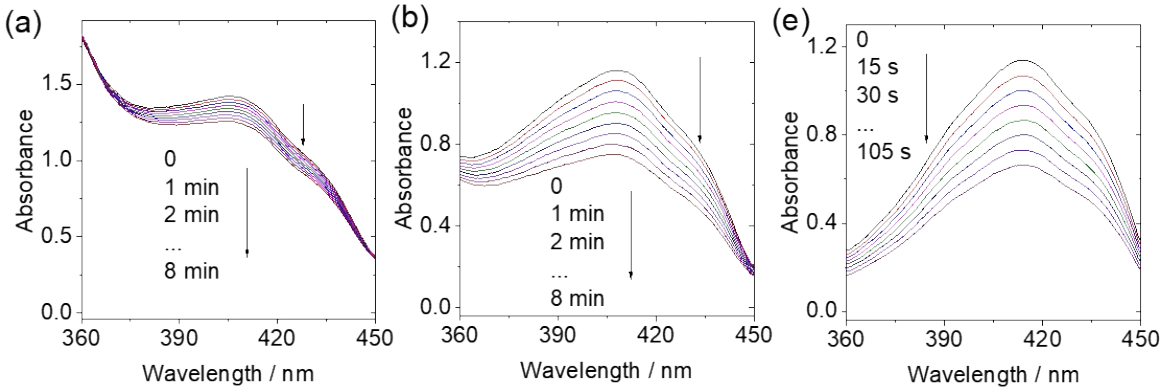

Fig. S20. The change of the UV-Vis absorption spectra of the compounds with the time after the addition of DPBF. (a) **[Ir-2ENR]PF_6** (b) **[Ir-3ENR]PF_6** in CH_3CN and the standard compound (c) methylene blue in DCM. λ_{ex} = 610 nm.

Additional Biological Results

SKBR-3 Cell Studies

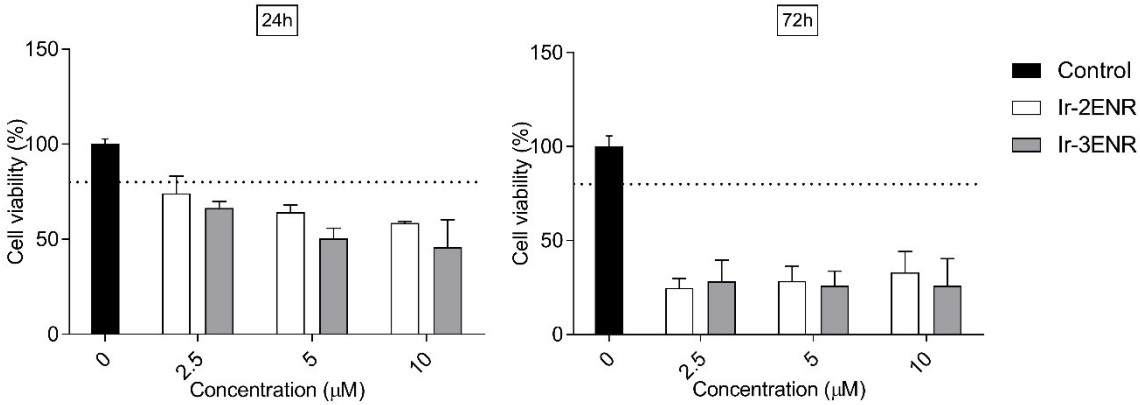

Fig. S21. Dark toxicity. Cell viability of SKBR-3 cells incubated in dark conditions with different concentrations of [Ir-2ENR]Cl and [Ir-3ENR]Cl (2.5, 5 and 10 μM), and a control (0 μM) at 24 h and 72 h. Experiments were done in triplicates.*p < 0.05

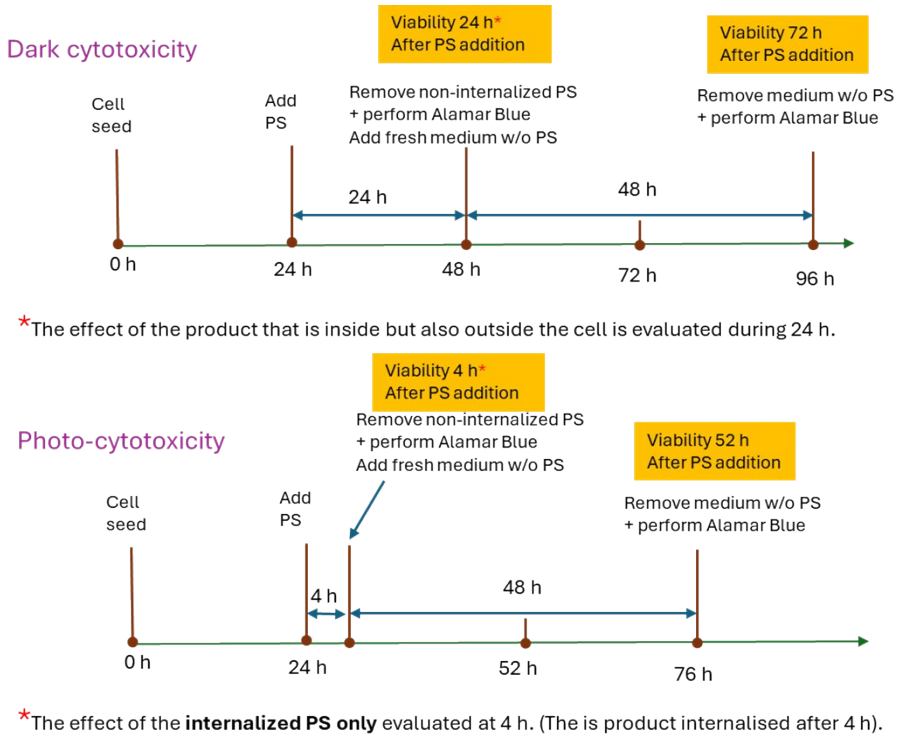

Fig. S22. Timeline for testing dark and photo toxicity of PSs against SKBR-3 cell line.

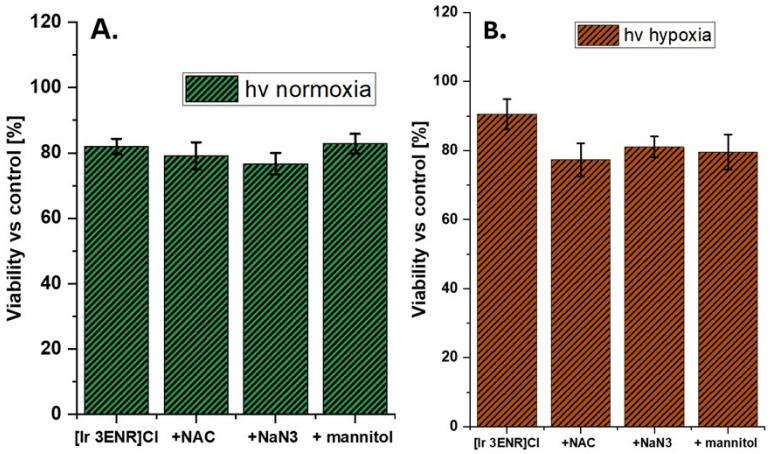

Fig. S23. The viability of MCF-7 cells after 24 h treatment with **[Ir-3ENR]Cl** (0.021 μM) without or with the antioxidants NAC (5 mM), NaN_3 (2 mM), or D-mannitol (50 mM) under normoxic (A) or hypoxic (B) conditions after irradiation (5 min, λ_{ex} 520 nm, 82 mJ cm^{-2}, 273.2 μWcm^{-2}).

References

1. K. A. Phillips, T. M. Stonelake, P. N. Horton, S. J. Coles, A. J. Hallett, S. P. O'Kell, J. M. Beames and S. J. A. Pope, Dual visible/NIR emission from organometallic iridium(III) complexes, *Journal of Organometallic Chemistry*, 2019, **893**, 11-20.
2. S. Ladouceur, D. Fortin and E. Zysman-Colman, Enhanced Luminescent Iridium(III) Complexes Bearing Aryltriazole Cyclometallated Ligands, *Inorganic Chemistry*, 2011, **50**, 11514-11526.
3. F. Monti, A. Baschieri, L. Sambri and N. Armaroli, Excited-State Engineering in Heteroleptic Ionic Iridium(III) Complexes, *Accounts of Chemical Research*, 2021, **54**, 1492-1505.
4. R. Bevernaegie, L. Marcélis, B. Laramée-Milette, J. De Winter, K. Robeyns, P. Gerbaux, G. S. Hanan and B. Elias, Trifluoromethyl-Substituted Iridium(III) Complexes: From Photophysics to Photooxidation of a Biological Target, *Inorganic Chemistry*, 2018, **57**, 1356-1367.
5. S. Admassie, O. Inganäs, W. Mammo, E. Perzon and M. R. Andersson, Electrochemical and optical studies of the band gaps of alternating polyfluorene copolymers, *Synthetic Metals*, 2006, **156**, 614-623.
6. H. Ferreira, M. M. Conradie and J. Conradie, Cyclic voltammetry data of polypyridine ligands and Co(II)-polypyridine complexes, *Data Brief*, 2019, **22**, 436-445.
7. C. Condon, R. Conway-Kenny, X. Cui, L. J. Hallen, B. Twamley, J. Zhao, G. W. Watson and S. M. Draper, Exploring the dark: detecting long-lived Nile Red 3ILCT states in Ru(ii) polypyridyl photosensitisers, *Journal of Materials Chemistry C*, 2021, **9**, 14573-14577.
8. V. V. Pavlishchuk and A. W. Addison, Conversion constants for redox potentials measured versus different reference electrodes in acetonitrile solutions at 25°C, *Inorganica Chimica Acta*, 2000, **298**, 97-102.